Cell Reports

Article

Secreted Phospholipase PLA2G2D Contributes to Metabolic Health by Mobilizing ω3 Polyunsaturated Fatty Acids in WAT

Graphical Abstract

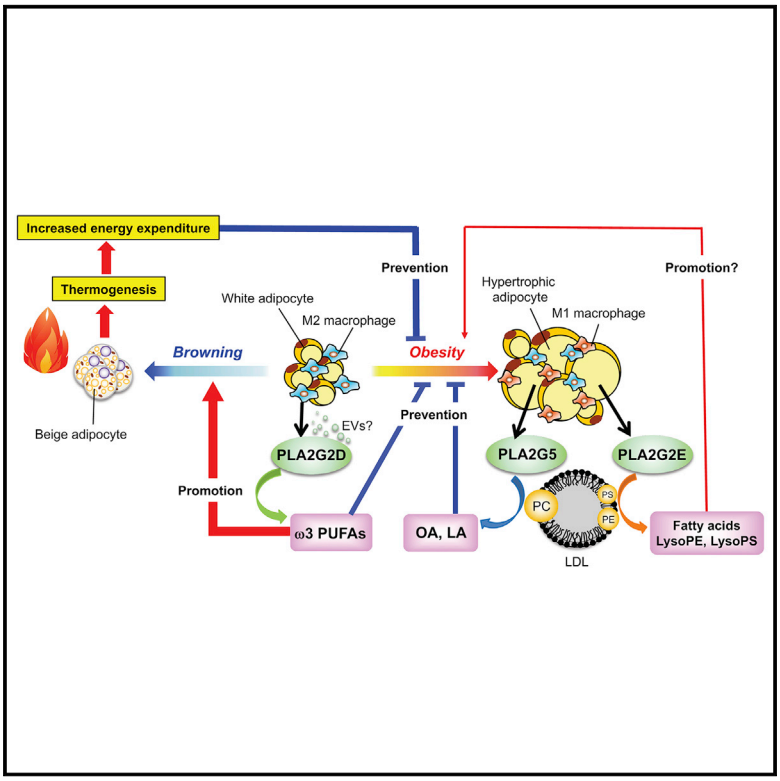

Authors

Hiroyasu Sato, Yoshitaka Taketomi, Yoshimi Miki, Remi Murase, Kei Yamamoto, Makoto Murakami

Correspondence

makmurak@m.u-tokyo.ac.jp

In Brief

Polyunsaturated fatty acids (PUFAs) confer health benefits by attenuating adipose tissue inflammation and by increasing thermogenesis through inducing beige adipocytes. Sato et al. find that the secreted phospholipase PLA2G2D in M2 macrophages supplies ω3 PUFAs that promote adipocyte browning partly via GPR120, thereby protecting against obesity-associated metabolic disorders.

Highlights

- PLA2G2D is expressed in M2 macrophages in WAT and downregulated in obesity
- Global and macrophage-specific PLA2G2D-null mice display increased obesity
- PLA2G2D deficiency perturbs adipocyte browning and adaptive thermogenesis
- PLA2G2D mobilizes a pool of ω3 polyunsaturated fatty acids in WAT

Sato et al., 2020, Cell Reports *31*, 107579
May 5, 2020
https://doi.org/10.1016/j.celrep.2020.107579

CellPress

Cell Reports

CellPress
OPEN ACCESS

Article

Secreted Phospholipase PLA2G2D Contributes to Metabolic Health by Mobilizing ω3 Polyunsaturated Fatty Acids in WAT

Hiroyasu Sato,[1,2] Yoshitaka Taketomi,[1,2] Yoshimi Miki,[1,2] Remi Murase,[1,2] Kei Yamamoto,[2,3] and Makoto Murakami[1,2,4,5,6,*]

[1]Laboratory of Microenvironmental and Metabolic Health Science, Center for Disease Biology and Integrative Medicine, Graduate School of Medicine, The University of Tokyo, 7-3-1 Hongo, Bunkyo-ku, Tokyo 113-8655, Japan
[2]Lipid Metabolism Project, Tokyo Metropolitan Institute of Medical Science, 2-1-6 Kamikitazawa, Setagaya-ku, Tokyo 156-8506, Japan
[3]Department of Bioscience and Bioindustry, Tokushima University, Tokushima 770-8506, Japan
[4]AMED-CREST, Japan Agency for Medical Research and Development, Tokyo 100-0004, Japan
[5]FORCE, Japan Agency for Medical Research and Development, Tokyo 100-0004, Japan
[6]Lead Contact
*Correspondence: makmurak@m.u-tokyo.ac.jp
https://doi.org/10.1016/j.celrep.2020.107579

SUMMARY

Polyunsaturated fatty acids (PUFAs) confer health benefits by preventing inflammation and obesity and by increasing thermogenesis in brown and beige adipocytes. As well as being supplied exogenously as nutrients, PUFAs are largely stored in membrane glycerophospholipids and released by phospholipase A_2s (PLA_2s). However, the molecular identity of the PLA_2 subtype(s) that supplies endogenous PUFAs for metabolic homeostasis remains unclear. Here we show that PLA2G2D, a secreted PLA_2 isoform, is constitutively expressed in M2-type macrophages in white adipose tissue (WAT) and shows a reciprocal correlation with obesity. Studies using global and macrophage-specific *Pla2g2d*-deficient mice reveal that PLA2G2D increases energy expenditure and thermogenesis by facilitating adipocyte browning, thereby ameliorating diet-induced obesity, insulin resistance, and WAT inflammation. Mechanistically, PLA2G2D constitutively supplies a pool of PUFAs, ω3 in particular, in WAT. Thus, our present findings underscore the contribution of the macrophage-driven PLA2G2D-ω3 PUFA axis to metabolic health.

INTRODUCTION

Metabolic syndrome is increasing at an explosive rate worldwide due to a pandemic of obesity, insulin resistance, and type 2 diabetes (Brestoff and Artis, 2015; Olefsky and Glass, 2010). White adipose tissue (WAT) is a principal lipid storage organ, whereas brown adipose tissue (BAT) consumes fuels for thermogenesis, thereby improving systemic metabolism (Lee et al., 2015; Uhm and Saltiel, 2015). Beige adipocytes, which are induced in WAT through a process termed "browning," have recently been attracting attention as another class of adipocytes that promote adaptive thermogenesis in response to cold exposure, physical exercise, and dietary intervention (Boström et al., 2012; Harms and Seale, 2013; Hui et al., 2015; Lee et al., 2015; Roberts et al., 2014; Rosenwald et al., 2013; Suárez-Zamorano et al., 2015). Accordingly, activation of brown and beige adipocytes could be an attractive therapeutic strategy against obesity and related metabolic complications (Hanssen et al., 2015). Whereas adipose tissue inflammation with recruitment of inflammatory cells including M1-type macrophages is tightly linked to insulin resistance, M2-type macrophages in concert with type 2 immunity attenuate obesity-associated inflammation and assist adipocyte browning, thereby exerting a beneficial impact on metabolism (Nguyen et al., 2011; Qiu et al., 2014; Rao et al., 2014). However, the mechanism whereby M2-type macrophages promote adipocyte browning still remains incompletely understood.

The quality of lipids is a critical determinant of various biological responses including metabolic diseases. Sustained elevation of saturated fatty acids (SFAs), such as palmitic acid (C16:0), causes lipotoxicity leading to chronic inflammation and insulin resistance, whereas unsaturated fatty acids counter this process by increasing membrane fluidity, acting as lipokines, or interacting with lipid-sensing receptors (Cao et al., 2008; Holzer et al., 2011). Arachidonic acid (AA; C20:4), an ω6 polyunsaturated fatty acid (PUFA), is metabolized to a class of lipid mediators (called eicosanoids) including prostaglandins (PGs) and leukotrienes (LTs), which diversely affect inflammation and metabolism (Li et al., 2015; Vegiopoulos et al., 2010). ω3 PUFAs, including eicosapentaenoic acid (EPA; C20:5) and docosahexaenoic acid (DHA; C22:6), serve as precursors of anti-inflammatory lipid mediators such as resolvins and protectins (Serhan, 2014), and also act by themselves as ligands for fatty-acid-sensing plasma membrane (e.g., GPR120) and nuclear (e.g.,

peroxisome proliferator-activated receptor [PPAR]) receptors, which improve metabolic homeostasis not only by attenuating adipose tissue inflammation but also by promoting adipocyte browning and thereby thermogenesis (Ichimura et al., 2012; Oh et al., 2010, 2014; Quesada-López et al., 2016; Syed et al., 2018; Yan et al., 2013). Moreover, recent studies have identified unusual fatty acid metabolites that control the thermogenic function of brown and beige adipocytes (Kim et al., 2017; Long et al., 2016; Lynes et al., 2017).

In a physiological state, a large fraction of PUFAs are incorporated into the *sn*-2 position of membrane phospholipids and released by phospholipase A_2 (PLA_2) enzymes (Murakami, 2017). Besides several intracellular PLA_2s or related lipases that have been implicated in metabolic regulation (Haemmerle et al., 2006; Mancuso et al., 2010; Peña et al., 2016; Tian et al., 2010), secreted PLA_2s ($sPLA_2$s) have recently emerged as a class of metabolic coordinators that can manipulate extracellular phospholipid metabolism in response to given microenvironmental cues. PLA2G1B ($sPLA_2$-IB), a "digestive $sPLA_2$," is secreted from the pancreas into the intestinal lumen, where it digests dietary and biliary phosphatidylcholine (PC) to produce lysophosphatidylcholine (LPC), which promotes obesity and insulin resistance following prandial absorption (Labonté et al., 2010). PLA2G5 ($sPLA_2$-V) and PLA2G2E ($sPLA_2$-IIE), two "metabolic $sPLA_2$s," are induced in hypertrophic white adipocytes during obesity and distinctly regulate systemic metabolism by acting on different phospholipids in lipoproteins (Sato et al., 2014). However, the identity of the particular PLA_2 subtype(s) that endogenously supplies free PUFAs in adipose tissue for metabolic regulation remains unknown.

PLA2G2D ($sPLA_2$-IID) is expressed abundantly in the spleen and lymph nodes and attenuates Th1 and Th17 immune responses by mobilizing anti-inflammatory ω3 PUFA metabolites (Miki et al., 2013, 2016). Interestingly, a polymorphism in the human *PLA2G2D* gene is linked to body weight changes in patients with chronic lung disease (Takabatake et al., 2005). Moreover, our recent microarray analysis using mouse WAT has revealed that, along with the *upregulated* $sPLA_2$s (PLA2G5 and PLA2G2E), PLA2G2D is found to be one of the most *downregulated* lipases during the onset of obesity (Sato et al., 2014), suggesting a potential contribution of PLA2G2D to metabolic regulation. Here we show that PLA2G2D is enriched in M2-type macrophages in WAT, promotes adipocyte browning, puts a brake on adipose tissue inflammation, and thereby counteracts diet-induced metabolic disorders by supplying a pool of PUFAs, ω3 in particular, with subsequent metabolic benefits. Thus, this study has identified a particular PLA_2 that lies upstream of the ω3 PUFA receptor GPR120 (fatty acid receptor 4) in the context of metabolic regulation.

RESULTS

M2-type Macrophages in WAT Constitutively Express PLA2G2D

Heatmap visualization of the expression of lipase-related genes in visceral WAT (vWAT) of C57BL/6 mice fed a high-fat diet (HFD; CLEA high-fat diet 32 [fat calorie 60%]) in comparison with those fed a standard low-fat diet (LFD; CLEA rodent diet CE-2 [fat 4.8%]) for 20 weeks (GEO: GSE56038) revealed that *Pla2g2d* was one of the most downregulated lipases in obese vWAT (Figure S1A) (Sato et al., 2014). Quantitative RT-PCR confirmed that, in addition to lymphoid organs (Miki et al., 2013, 2016), *Pla2g2d* was substantially detected in vWAT of LFD-fed mice and decreased after HFD feeding, whereas its expression was very low in BAT, heart, liver, and skeletal muscle regardless of diet (Figure 1A). This expression pattern of *Pla2g2d* in vWAT was in contrast to that of *Pla2g2e* and *Pla2g5*, whose expression levels were low on an LFD and markedly induced after HFD feeding (Figure 1B). Indeed, under LFD conditions, *Pla2g2d* is a major $sPLA_2$ expressed in vWAT and more abundantly in subcutaneous WAT (sWAT), and its steady-state expression in vWAT of LFD-fed mice was comparable to the induced expression of *Pla2g2e* and *Pla2g5* in HFD-fed mice (Figures 1B, 1C, and S1B). Moreover, *Pla2g2d* expression in vWAT and sWAT was markedly lower in genetically obese *ob/ob* mice than in control mice (Figure 1C).

When vWAT was separated into adipocytes and the stromal vascular fraction (SVF), *Pla2g2d* expression was exclusively enriched in the SVF and decreased after HFD feeding for 20 weeks (Figure 1D). Further sorting of SVF cells into $Sca1^+CD11b^-CD45^-$ preadipocyte-rich and $Sca1^-CD11b^+CD45^+$ hematopoietic cell-rich fractions revealed that *Pla2g2d* was expressed mainly in the latter (Figures 1E and S1C). After sorting of F4/80-gated macrophages within the SVF, *Pla2g2d* expression was distributed in $CD11c^{lo}CD206^{hi}$ M2-like macrophages in marked preference to $CD11c^{hi}CD206^{lo}$ M1-like macrophages and decreased after HFD feeding (Figures 1F and S1D). In agreement, immunoreactive PLA2G2D protein was located almost exclusively in $F4/80^+CD206^+$ macrophages in vWAT (Figure 1G). Moreover, when macrophage colony-stimulating factor (M-CSF)-driven bone-marrow-derived macrophages (BMDMs; M0, which is M2 like) were polarized into M1- or M2-type macrophages *ex vivo* by interferon-γ (IFN-γ) + lipopolysaccharide (LPS) and interleukin-4 (IL-4), respectively, *Pla2g2d* was expressed in the order M2 > M0 > M1 (Figure 1H). Proper polarization of BMDMs to M1- and M2-type macrophages in this setting was validated by the expression of their signature markers *Nos2* and *Cd206*, respectively (Figure S1E). Furthermore, *Pla2g2d* expression in BMDMs was decreased after treatment with palmitic acid (Figure 1I), an SFA that promotes M1 polarization of macrophages (Figure S1F). These results indicate that PLA2G2D is enriched in M2-type macrophages in WAT of lean mice and downregulated during the process of obesity.

Exacerbated Diet-Induced Obesity and Insulin Resistance in HFD-Fed *Pla2g2d*$^{-/-}$ Mice

To assess the role of PLA2G2D in diet-induced obesity, we placed *Pla2g2d*$^{-/-}$ mice (Miki et al., 2013) and their littermate controls on an HFD. We found that obesity and weight gain were significantly greater in HFD-fed *Pla2g2d*$^{-/-}$ mice than in *Pla2g2d*$^{+/+}$ mice (Figures 2A and 2B), despite similar food intake between the genotypes (Figure S2A). The proportions of total, visceral, and subcutaneous fats (Figure 2C) and adipocyte size in vWAT (Figures 2D and S2B) were significantly greater in *Pla2g2d*$^{-/-}$ mice than in *Pla2g2d*$^{+/+}$ mice after HFD feeding for 20 weeks. Plasma levels of leptin (Figure 2E) and insulin

CellPress
OPEN ACCESS

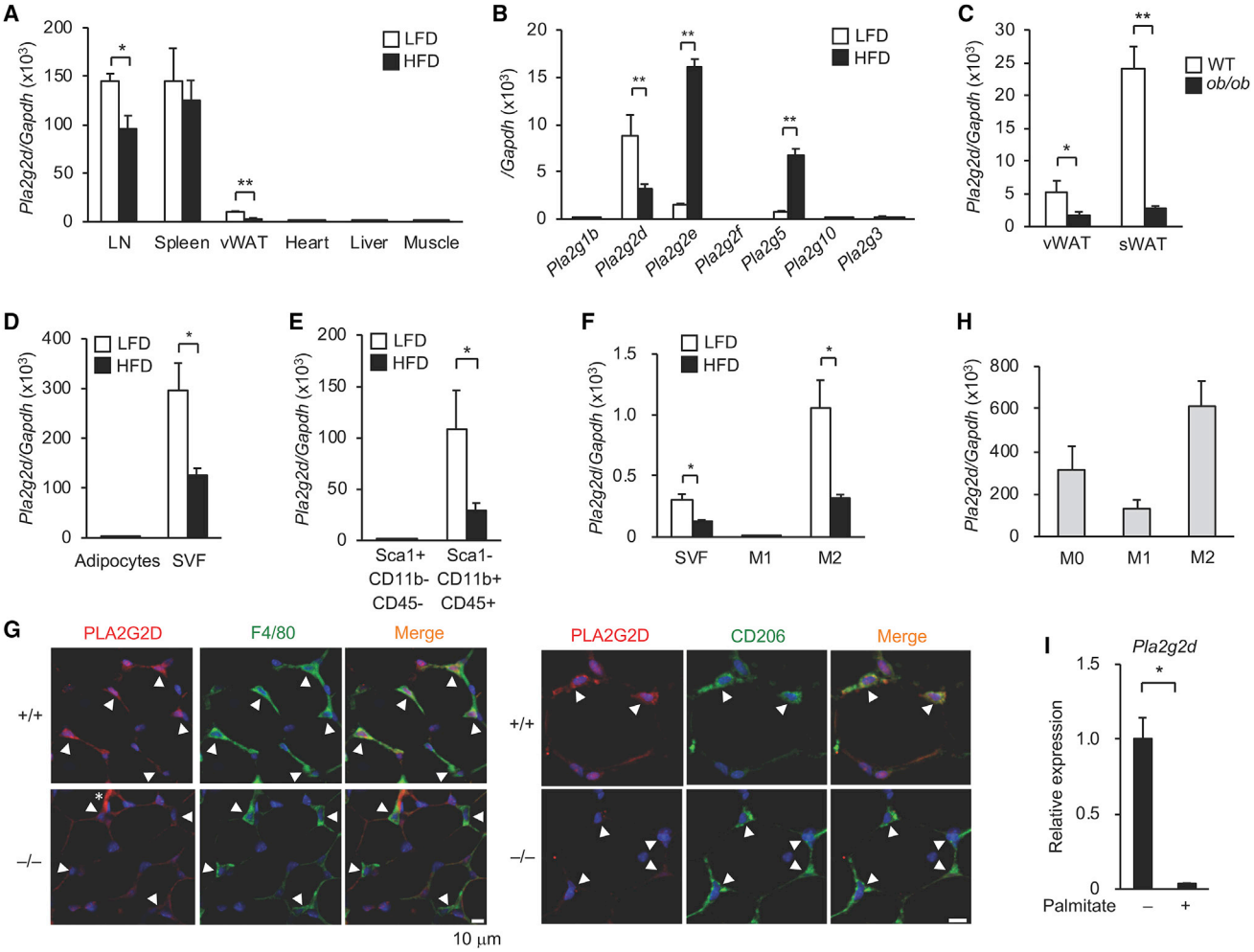

Figure 1. *Pla2g2d* Is Expressed in M2 Macrophages in WAT

(A and B) Quantitative RT-PCR of *Pla2g2d* mRNA in various tissues (A) and various $sPLA_2$ mRNAs in vWAT (B) from C57BL/6 mice fed an LFD (n = 4) or HFD (n = 5) for 20 weeks. Expression levels were normalized against *Gapdh*. LN, lymph node.

(C) Quantitative RT-PCR of *Pla2g2d* mRNA in vWAT and sWAT of 12-week-old *ob/ob* mice and age-matched control (wild type [WT]) C57BL/6 mice (n = 4).

(D–F) Quantitative RT-PCR of *Pla2g2d* mRNA in adipocytes and SVF (n = 3) (D), in $Sca1^+CD11b^-CD45^-$ (preadipocyte-rich) and $Sca1^-CD11b^+CD45^+$ (hematopoietic cell-rich) fractions sorted from SVF by fluorescence-activated cell sorting (FACS) (n = 3) (E), and in $CD11c^{hi}CD206^{lo}$ M1 macrophages and $CD11c^{lo}CD206^{hi}$ M2 macrophages sorted from F4/80-gated SVF by FACS (n = 3) (F) from vWAT of LFD- or HFD-fed mice. Representative FACS profiles for (E) and (F) are shown in Figures S1C and S1D.

(G) Immunofluorescence microscopy of PLA2G2D, F4/80, and CD206 in vWAT of LFD-fed C57BL/6 mice. PLA2G2D was colocalized in $F4/80^+$ or $CD206^+$ macrophages (arrowheads) in $Pla2g2d^{+/+}$ mice, whereas it was scarcely stained in $Pla2g2d^{-/-}$ mice (the asterisk indicates non-specific staining).

(H) Quantitative RT-PCR of *Pla2g2d* mRNA in BMDMs cultured for 24 h in the absence (M0) or presence of IFN-γ + LPS (M1) or IL-4 (M2) (n = 9).

(I) Expression of *Pla2g2d* mRNA in BMDMs cultured for 24 h in the presence (+) or absence (–) of 100 μM palmitic acid, the expression without palmitic acid being regarded as 1 (n = 4).

Data are compiled from two experiments (B and H) or from one representative experiment (A, C, E–G, and I). Mean ± SEM, *$p < 0.05$, **$p < 0.01$.

See also Figure S1.

(Figure 2F) were elevated in HFD-fed $Pla2g2d^{-/-}$ mice relative to $Pla2g2d^{+/+}$ mice. Moreover, HFD-fed, but not LFD-fed, $Pla2g2d^{-/-}$ mice had a higher steady-state blood glucose level and displayed greater insulin resistance in an insulin tolerance test (ITT) than did replicate $Pla2g2d^{+/+}$ mice (Figure 2G), although glucose clearance demonstrated by a glucose tolerance test (GTT) was similar between the genotypes (Figure S2C). In agreement with the aggravated insulin intolerance (Figure 2G), insulin-stimulated Akt phosphorylation tended to be reduced in vWAT of $Pla2g2d^{-/-}$ mice relative to $Pla2g2d^{+/+}$ mice (Figure S2D). Although two diet-induced $sPLA_2$s, PLA2G5 and PLA2G2E, exert their metabolic effects by hydrolyzing lipoprotein phospholipids (Sato et al., 2014), neither of the lipid profiles in plasma lipoproteins (Figure S2E) nor the phospholipid levels in low-density lipoprotein (LDL) and high-density lipoprotein (HDL) (Figure S2F) were altered in $Pla2g2d^{-/-}$ mice regardless of diet.

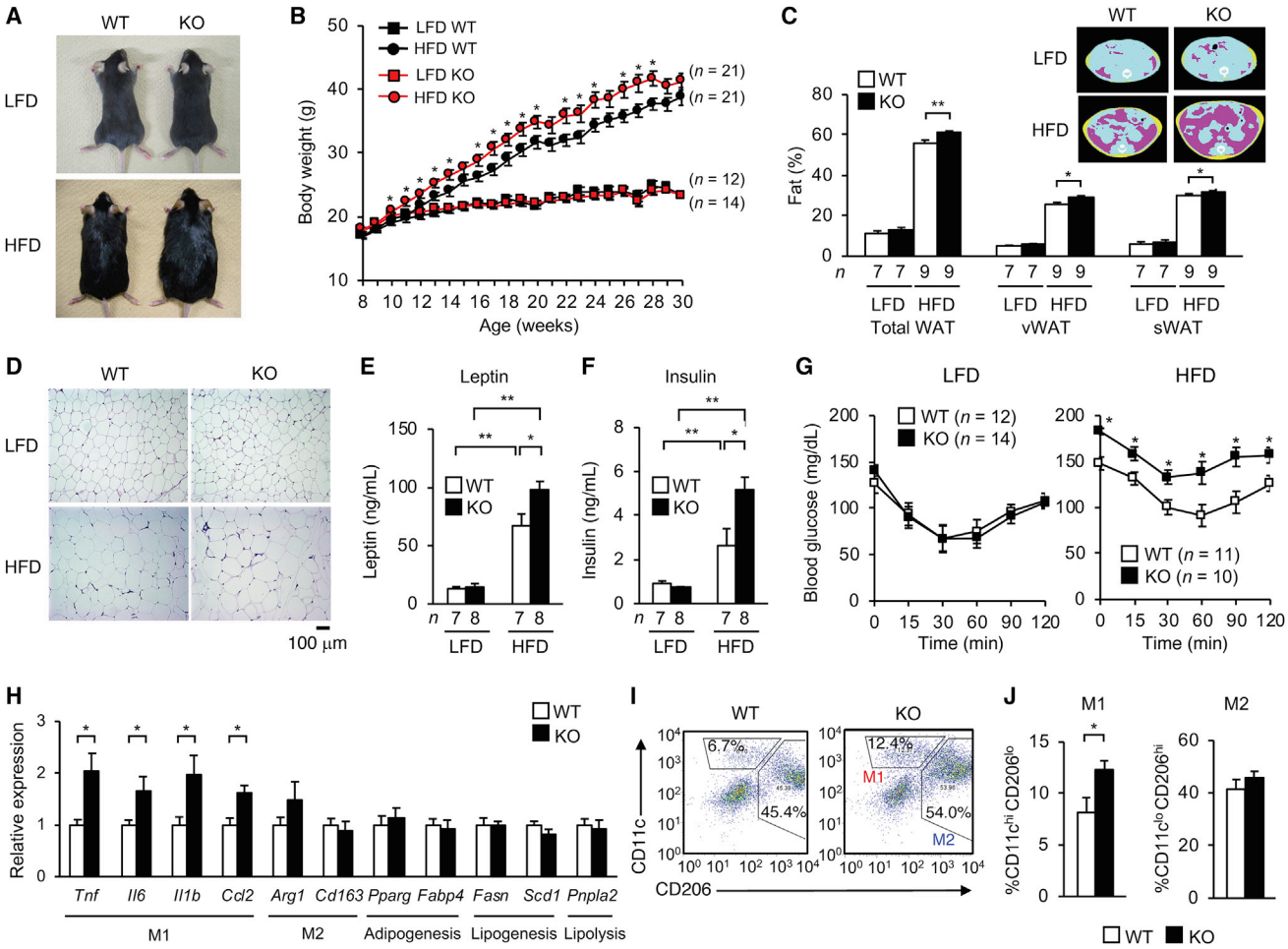

Figure 2. Increased Diet-Induced Obesity in *Pla2g2d*$^{-/-}$ Mice

(A) Gross appearance of *Pla2g2d*$^{+/+}$ (WT) and *Pla2g2d*$^{-/-}$ (KO) mice fed an LFD or HFD for 20 weeks.

(B) Body weights of WT and KO mice placed on an LFD or HFD for the indicated periods.

(C) Computed tomography (CT) analysis of fat volumes in WT and KO mice fed an LFD or HFD for 20 weeks. Yellow and purple areas indicate sWAT and vWAT, respectively (inset).

(D) Hematoxylin-eosin staining of vWAT of WT and KO mice fed an LFD or HFD for 26 weeks (scale bar, 100 μm).

(E and F) Plasma leptin (E) and insulin (F) levels in LFD- or HFD-fed WT and KO mice.

(G) ITT using LFD- or HFD-fed WT and KO mice after fasting for 6 h.

(H) Quantitative RT-PCR of various genes in vWAT of LFD- or HFD-fed WT and KO mice, with expression in LFD-fed WT mice, normalized against *Rn18s*, being regarded as 1 (n = 7).

(I and J) Flow cytometry of M1- and M2-type macrophages in vWAT of HFD-fed WT and KO mice. Representative FACS profiles (I) and quantified values (n = 5) (J) of M1- and M2-type macrophages are shown.

Data are compiled from one (I and J), two (C, E, F, and H), or three (B and G) experiments. Images in (A), (C), and (D) are representative of two experiments. In (B), (C), and (E)–(G), sample sizes (n) are indicated in the figure. Mean ± SEM, *$p < 0.05$, **$p < 0.01$.

See also Figures S2 and S3.

The expression levels of *Pla2g5* and *Pla2g2e* in vWAT were not affected by *Pla2g2d* deficiency (Figure S2G). These results suggest that the metabolic effects of PLA2G2D are not dependent on lipoprotein phospholipid hydrolysis and not compensated by other adipose tissue sPLA$_2$s.

Quantitative RT-PCR of vWAT revealed that, although the expression levels of adipogenic (*Pparg* and *Fabp4*), lipogenic (*Fasn* and *Scd1*), or lipolytic (*Pnpla2*) genes were not affected by *Pla2g2d* deficiency, those of pro-inflammatory M1 macrophage markers (*Tnf*, *Il6*, *Il1b*, and *Ccl2*), but not anti-inflammatory M2 macrophage markers (*Arg1* and *Cd206*), were consistently elevated in HFD-fed *Pla2g2d*$^{-/-}$ mice relative to *Pla2g2d*$^{+/+}$ mice (Figure 2H). Moreover, flow cytometry of F4/80-gated macrophages in vWAT revealed an increased proportion of CD11c^{hi}CD206^{lo} M1-like macrophages and an unaltered proportion of CD11c^{lo}CD206^{hi} M2-like macrophages in HFD-fed *Pla2g2d*$^{-/-}$ mice relative to *Pla2g2d*$^{+/+}$ mice (Figures 2I and 2J), suggesting an increased M1/M2 ratio in the absence of PLA2G2D. To assess whether these alterations already occurred at an earlier period of diet-induced obesity, we examined the

inflammatory status at 6 weeks after HFD, at which time the expression level of *Pla2g2d* in vWAT of HFD-fed mice still remained high (Figure S3A) and *Pla2g2d*$^{-/-}$ mice began to gain more body weight than did *Pla2g2d*$^{+/+}$ mice (Figure 2B). Trends toward an increased proportion of CD11c^{hi}CD206^{lo} M1-like macrophages (Figures S3B and S3C) and an increased expression of *Il1b* (Figure S3D) were already evident in vWAT of *Pla2g2d*$^{-/-}$ mice after HFD feeding for 6 weeks, although the M1/M2 ratio of WAT macrophages prior to HFD feeding was similar between the genotypes (Figures S3B and S3C). Additionally, the expression of pro-inflammatory genes (such as *Ifng*) in regional lymph nodes, where PLA2G2D was highly expressed (Figure 1A), was significantly greater in *Pla2g2d*$^{-/-}$ mice than in *Pla2g2d*$^{+/+}$ mice after HFD feeding for 6 weeks (Figure S3E), suggesting that the absence of PLA2G2D exacerbates HFD-induced inflammation in the lymph nodes as well. In agreement with these *in vivo* observations, when BMDMs were polarized into M1- or M2-type macrophages *ex vivo*, expression of the M1 marker *Tnf* was higher in *Pla2g2d*$^{-/-}$ cells than in *Pla2g2d*$^{+/+}$ cells, whereas that of the M2 marker *Cd206* was similar between the genotypes (Figure S3F).

In contrast to the notable alterations in vWAT and lymph nodes, HFD-induced hepatic steatosis in terms of liver histology (Figure S3G), plasma level of alanine aminotransferase (ALT; a marker of liver damage) (Figure S3H), and hepatic expression of genes involved in lipid metabolism and inflammation (Figure S3I) did not differ significantly between the genotypes, probably because *Pla2g2d* expression in the liver was very low (Figure 1A). Collectively, global ablation of *Pla2g2d* exacerbates diet-induced obesity, insulin resistance, and adipose tissue inflammation.

Macrophage-Specific *Pla2g2d* Ablation Recapitulates the Metabolic Phenotypes

To address whether PLA2G2D expressed in M2-like macrophages could indeed participate in metabolic regulation, we crossed *Pla2g2d*$^{fl/fl}$ mice with *Lys2-Cre* transgenic mice, which have frequently been used for conditional deletion of a target gene in the myeloid cell lineage, particularly in monocytes and macrophages (Figure S4A). Conditional deletion of *Pla2g2d* was verified by PCR genotyping (Figure S4B) and by quantitative RT-PCR, in which *Pla2g2d* expression was largely even if not solely abrogated in vWAT and sWAT, as well as in IL-4-treated, M2-polarized BMDMs, prepared from *Pla2g2d*$^{fl/fl}$*Lys2-Cre* mice (Figure S4C). Because *Pla2g2d* expression is enriched in macrophages and dendritic cells (Miki et al., 2013, 2016) and very low in Ly6G1^{hi}CD11b^{+} granulocytes (Figures S4D and S4E), we reasoned that the phenotypes observed in *Pla2g2d*$^{fl/fl}$*Lys2-Cre* mice could be attributed largely to the lack of PLA2G2D in the monocyte/macrophage lineage.

When fed an HFD, *Pla2g2d*$^{fl/fl}$*Lys2-Cre* mice appeared more obese (Figure 3A), displayed greater weight gain (Figure 3B), and accumulated more visceral, subcutaneous, and total fats (Figure 3C) than did control *Pla2g2d*$^{fl/fl}$ mice. Histologically, vWAT of HFD-fed *Pla2g2d*$^{fl/fl}$*Lys2-Cre* mice had larger adipocytes with more crown-like structures (an indicator of macrophage infiltration) than that of replicate *Pla2g2d*$^{fl/fl}$ mice (Figure 3D). Plasma leptin and insulin levels were higher (Figures 3E and 3F) and insulin sensitivity as assessed by ITT was lower (Figure 3G) in HFD-fed *Pla2g2d*$^{fl/fl}$*Lys2-Cre* mice than in *Pla2g2d*$^{fl/fl}$ mice, although glucose clearance as assessed by GTT was similar in both genotypes (Figure S4F). Expression levels of M1 macrophage markers were elevated, whereas those of M2 macrophage markers were unchanged or decreased, in vWAT of HFD-fed *Pla2g2d*$^{fl/fl}$*Lys2-Cre* mice relative to *Pla2g2d*$^{fl/fl}$ mice (Figure 3H). There was no alteration of adipogenic, lipogenic, or lipolytic genes in vWAT of *Pla2g2d*$^{fl/fl}$*Lys2-Cre* mice (Figure 3H). Thus, the phenotypes resulting from macrophage-specific *Pla2g2d* ablation largely recapitulate those resulting from its global deficiency.

Impaired Adipocyte Browning and Adaptive Thermogenesis in *Pla2g2d*$^{-/-}$ Mice

Besides the metabolic complications described above, we noticed that *Pla2g2d*$^{-/-}$ mice had significantly lower O_2 and CO_2 consumption than did *Pla2g2d*$^{+/+}$ mice under HFD and even normal LFD conditions (Figures 4A and S5A). A steady-state reduction of O_2 consumption was also evident in *Pla2g2d*$^{fl/fl}$*Lys2-Cre* mice relative to *Pla2g2d*$^{fl/fl}$ mice (Figure 4B). These results indicate that energy expenditure under normal housing conditions was reduced by the absence of PLA2G2D in macrophages, an event that had not been observed in other sPLA$_2$-knockout (KO) strains (Sato et al., 2014). However, neither respiratory quotient (Figure S5B) nor locomotion (Figure S5C) was affected by global or macrophage-specific *Pla2g2d* deletion. Notably, the expression level of *Ucp1*, a key marker of non-shivering thermogenesis that uncouples oxidative phosphorylation from energy production to heat generation (Kozak, 2010), as well as several mitochondrial thermogenic markers such as *Cidea* and *Cox8b*, tended to be lower in vWAT of *Pla2g2d*$^{-/-}$ or *Pla2g2d*$^{fl/fl}$*Lys2-Cre* mice than in that of respective control mice under normal housing conditions (Figure S5D). We therefore speculated that *Pla2g2d*$^{-/-}$ mice might have some alterations in the process of thermogenesis, thus affecting energy expenditure.

β_3-adrenergic signaling in response to cold stimulation upregulates the expression of thermogenic genes in WAT, a process known as "browning" (or "beiging") (Cao et al., 2011; Nedergaard and Cannon, 2014). Animals with impairment of beige adipocyte function are vulnerable to metabolic challenges (Cohen et al., 2014; Jun et al., 2018). We therefore examined whether cold-induced adipocyte browning would be perturbed by *Pla2g2d* deficiency by placing *Pla2g2d*$^{-/-}$ and *Pla2g2d*$^{+/+}$ mice in a thermoneutral environment at 30°C for 2 days and then transferring them to a cold environment at 4°C for up to 5 days. After this temperature shift, adipocytes in vWAT and sWAT of *Pla2g2d*$^{+/+}$ mice became smaller and more multilocular, expressing higher levels of immunoreactive UCP1 protein (Figure 4C), a characteristic feature of adipocyte browning. Strikingly, these cold-induced processes were markedly perturbed in *Pla2g2d*$^{-/-}$ mice (Figure 4C). Consistently, cold exposure resulted in robust upregulation of *Ucp1* and other mitochondrial thermogenic markers in vWAT and even more in sWAT of *Pla2g2d*$^{+/+}$ mice, whereas *Pla2g2d* deficiency substantially attenuated these cold-induced responses (Figure 4D). Moreover, after administration of CL316,243, a β_3-adrenergic receptor agonist, there was marked upregulation of *Ucp1* and other

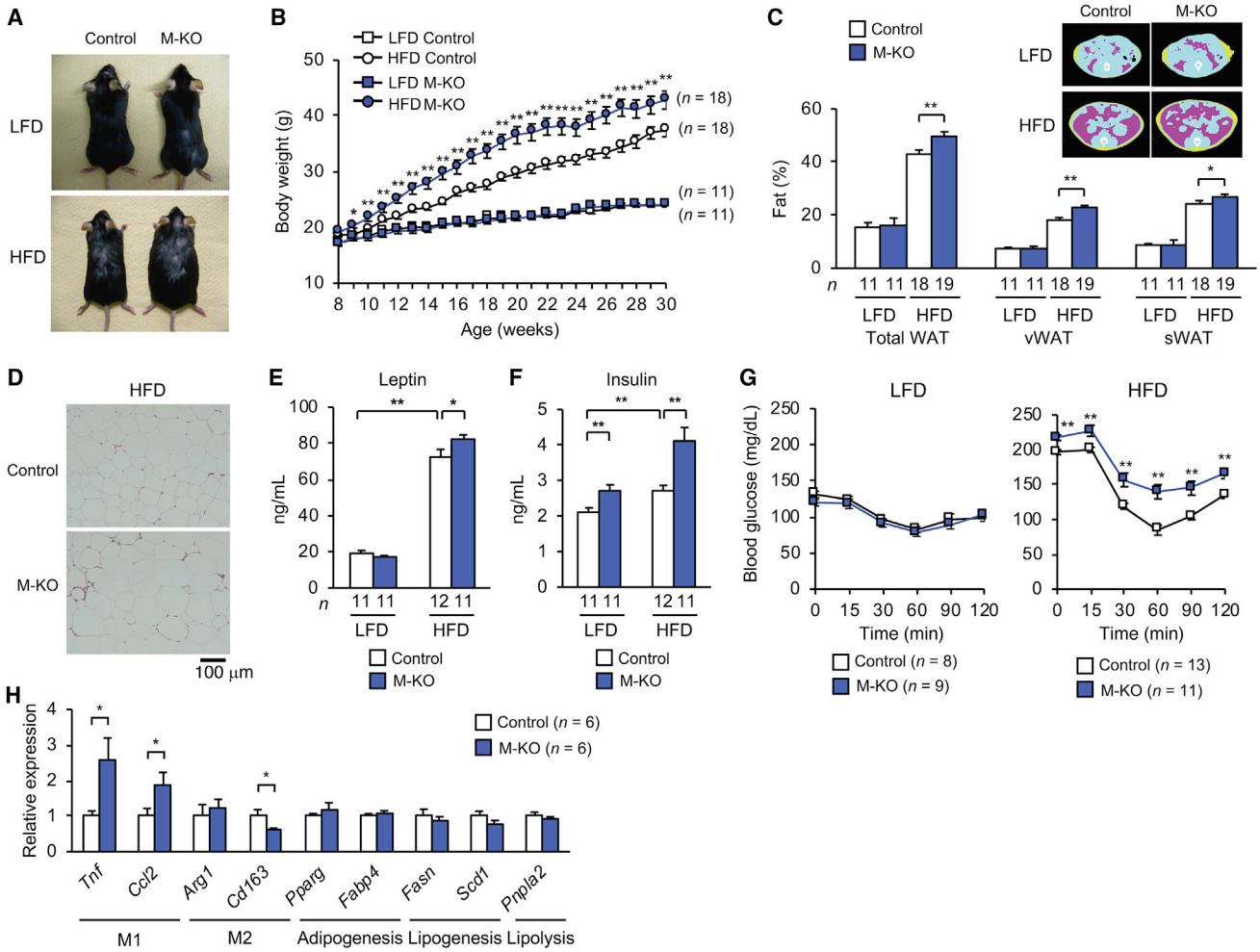

Figure 3. Increased Diet-Induced Obesity in Macrophage-Specific *Pla2g2d*-Null Mice

(A) Gross appearance of *Pla2g2d*$^{fl/fl}$ (control) and macrophage-specific *Pla2g2d*-deficient (*Pla2g2d*$^{fl/fl}$*Lys2-Cre*; M-KO) mice fed an LFD or HFD for 20 weeks.

(B) Body weights of control and M-KO mice placed on an LFD or HFD for the indicated periods.

(C) CT analysis of fat volumes in control and M-KO mice fed an LFD or HFD for 26 weeks. Yellow and purple areas indicate sWAT and vWAT, respectively (inset).

(D) Hematoxylin-eosin staining of vWAT of control and M-KO mice fed an HFD for 26 weeks (scale bar, 100 μm).

(E and F) Plasma levels of leptin (E) and insulin (F) in LFD- or HFD-fed control and M-KO mice.

(G) ITT using LFD- or HFD-fed control and M-KO mice after fasting for 6 h.

(H) Quantitative RT-PCR of various genes in vWAT of HFD-fed control and M-KO mice, with the expression in control mice, normalized with *Rn18s*, being regarded as 1.

Data are compiled from two (E–G) or three (B and C) experiments. Images in (A), (C), and (D) are representative of two or three experiments. Sample sizes (n) are indicated in the figure. Mean ± SEM, *p < 0.05, **p < 0.01.

See also Figure S4.

markers of thermogenesis in vWAT and more robustly in sWAT of *Pla2g2d*$^{+/+}$ mice, whereas these responses were again impaired in *Pla2g2d*$^{-/-}$ mice (Figure 4E). Likewise, cold- or CL316,243-induced upregulation of *Ucp1* was substantially mitigated in sWAT of *Pla2g2d*$^{fl/fl}$*Lys2-Cre* mice (Figures S5E and S5F). CL316,243 did not affect *Pla2g2d* expression in either vWAT or sWAT (Figure S5G). In contrast, expression levels of various thermogenic markers in interscapular BAT under normal (23°C), thermoneutral (30°C), and cold (4°C) conditions were barely affected by *Pla2g2d* deletion (Figure S5H), likely because of low *Pla2g2d* expression in BAT (Figure 1A).

Reflecting the impaired adipocyte browning and thermogenesis resulting from *Pla2g2d* ablation, the cold-induced decrease of rectal temperature was significantly greater in *Pla2g2d*$^{-/-}$ mice than in *Pla2g2d*$^{+/+}$ mice (Figure 4F). Moreover, cold-induced expression of fibroblast growth factor 21 (FGF21), an endocrine hormone that plays an intermediate role in adipocyte browning (Fisher et al., 2012; Huang et al., 2017; Lee et al., 2014), was lower in the plasma (Figure 4G) and in vWAT and sWAT (Figure 4H) of *Pla2g2d*$^{-/-}$ mice than in *Pla2g2d*$^{+/+}$ mice. Collectively, these results suggest that PLA2G2D promotes cold-induced adipocyte browning and adaptive thermogenesis, which could

CellPress
OPEN ACCESS

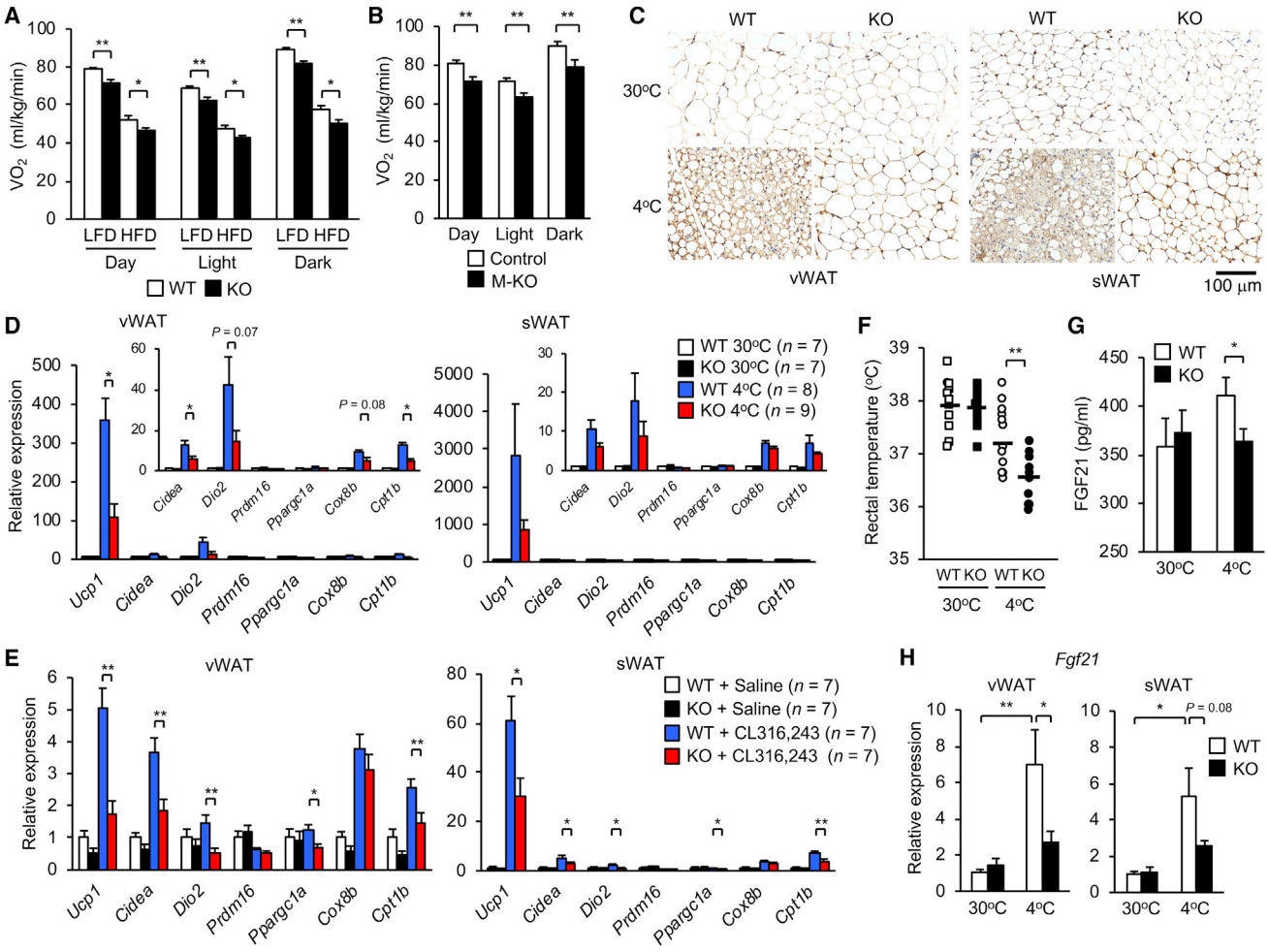

Figure 4. Decreased Adipocyte Browning and Thermogenesis Resulting from *Pla2g2d* Deficiency

(A and B) Oxygen consumption in *Pla2g2d*$^{+/+}$ (WT) and *Pla2g2d*$^{-/-}$ (KO) mice fed an LFD (n = 4) or HFD (n = 7) for 26 weeks (A) or that of *Pla2g2d*$^{fl/fl}$ (control) and *Pla2g2d*$^{fl/fl}$*Lys2-Cre* (M-KO) mice maintained on an LFD (n = 6) (B) at 23°C.

(C) Immunostaining of UCP1 in vWAT and sWAT of WT and KO mice placed at 30°C for 2 days or at 4°C for an additional 5 days (scale bar, 100 μm).

(D and E) Quantitative RT-PCR of thermogenesis-related genes in vWAT and sWAT of WT and KO mice placed at 30°C for 2 days or at 4°C for an additional 5 days (D) or after treatment with CL316,243 (1 mg/kg body weight) or saline for 3 days at 23°C (E), with basal expression of each marker in WT mice at 30°C (D) or with saline treatment (E) being regarded as 1. Expression levels of several genes are magnified in the inset of (D).

(F) Rectal temperature of WT and KO mice placed at 30°C for 2 days or at 4°C for an additional 1 day (n = 13).

(G and H) FGF21 levels in plasma (n = 12) (G) and its mRNA expression in vWAT and sWAT (n = 9) (H) of WT and KO mice placed at 30°C for 2 days or at 4°C for an additional 5 days.

In (D), (E), and (H), the expression levels of individual genes were normalized with *Gapdh*. Data are compiled from two (A, B, D, and E) or three (F–H) experiments. Images in (C) are representative of two experiments. In (D) and (E), sample sizes (n) are indicated in the figure. Mean ± SEM, *p < 0.05, **p < 0.01.
See also Figure S5.

account, at least in part, for the exacerbated diet-induced obesity in *Pla2g2d*$^{-/-}$ mice. However, expression of neither *Prdm16*, a key transcription factor for beige adipocyte development (Cohen et al., 2014; Harms et al., 2014), nor type 2 cytokines (*Il4*, *Il5*, *Il13*, and *Il33*), which facilitate adipocyte browning (Lee et al., 2015; Uhm and Saltiel, 2015), in vWAT and sWAT was significantly affected by *Pla2g2d* ablation (Figures 4D, 4E, and S5I). Thus, during the process of WAT browning, PLA2G2D might participate in a step prior to FGF21 induction and beyond the core program for differentiation of beige adipocytes from committed progenitors or for propagation of type 2 immunity.

PLA2G2D Mobilizes PUFAs in WAT

Given that PLA2G2D is a phospholipase, we examined the profile of PLA_2-driven fatty acids and their metabolites in WAT by electrospray ionization mass spectrometry (ESI-MS/MS). Under steady-state LFD conditions, when *Pla2g2d* expression was high (Figure 1A), the WAT levels of free PUFAs including AA (C20:4), EPA (C20:5), and DHA (C22:6), but not palmitic acid (C16:0), stearic acid (C18:0), oleic acid (OA; C18:1), and linoleic acid (LA; C18:2), were significantly lower in *Pla2g2d*$^{-/-}$ mice than in *Pla2g2d*$^{+/+}$ mice (Figures 5A and 5B). Moreover, at an earlier time point of HFD feeding (6 weeks), when *Pla2g2d* expression

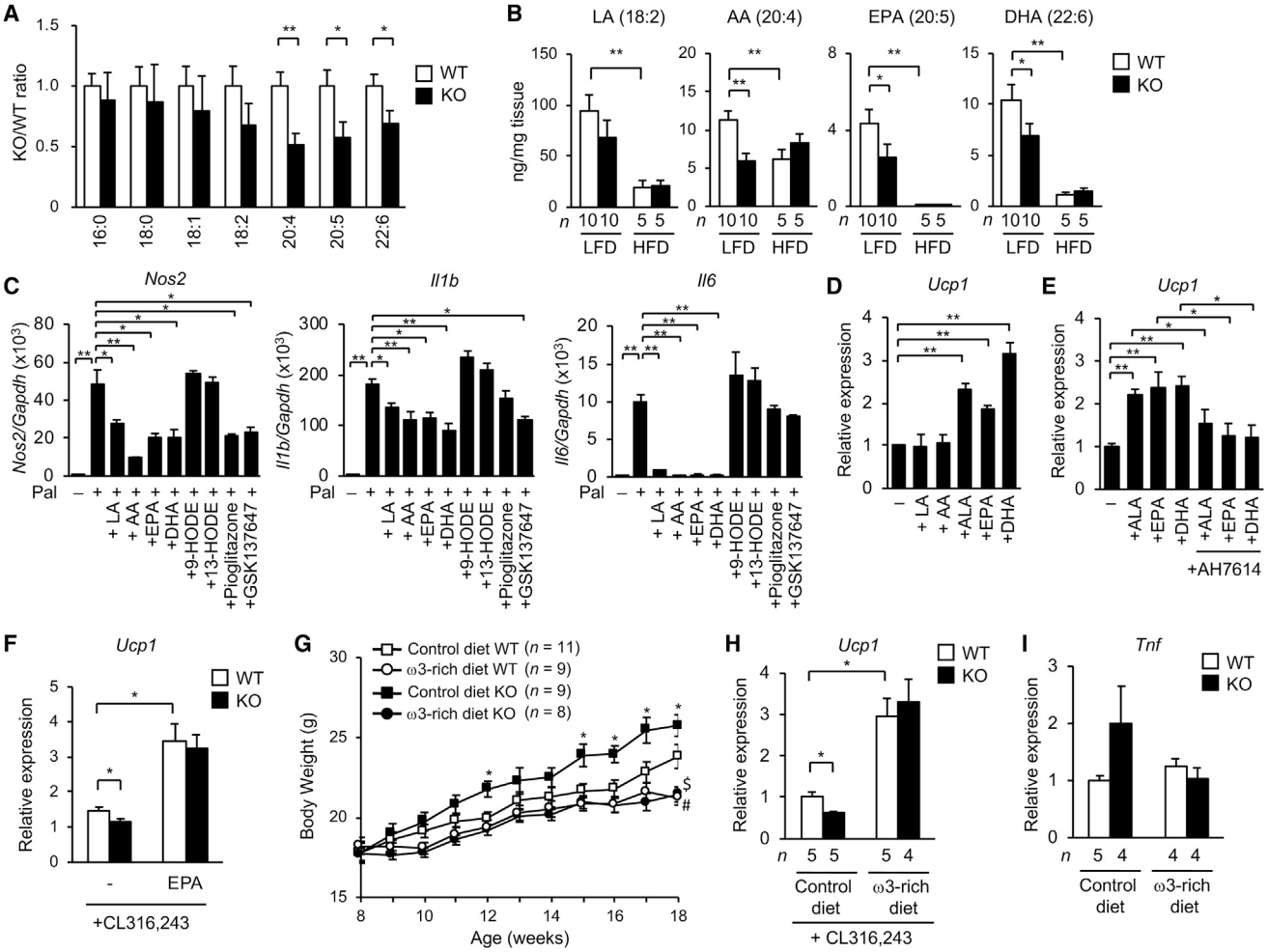

Figure 5. PLA2G2D Mobilizes PUFAs in WAT

(A and B) Lipidomics analyses of fatty acids in WAT of *Pla2g2d*$^{+/+}$ (WT) and *Pla2g2d*$^{-/-}$ (KO) mice placed on an LFD or HFD for 26 weeks (n = 10). Relative levels of fatty acids in WAT of LFD-fed mice, with values in WT mice being regarded as 1, are shown in (A), and quantified values (ng/mg tissue) of PUFAs under LFD or HFD conditions are shown in (B).

(C) Expression of inflammatory M1 markers in BMDMs after culture for 24 h with 100 μM palmitate in the presence or absence of 20 μM PUFAs, 10 μM 9- or 13-HODE, 50 μM GSK137647 (GPR120 agonist), or 10 μM pioglitazone (PPARγ agonist) (n = 3).

(D and E) Quantitative RT-PCR of *Ucp1* in *ex-vivo*-differentiated primary adipocytes after treatment for 24 h with various PUFAs (D) or with ω3 PUFAs in the presence or absence of the GPR120 antagonist AH7614 (E), with expression in the absence of PUFAs being regarded as 1 (n = 4).

(F) Quantitative RT-PCR of *Ucp1* in WAT explants obtained from WT and KO mice. The explants were cultured for 6 h with 1 μM CL316,243 in the presence or absence of 100 μM EPA (n = 10).

(G) Body weights of WT and KO mice placed on a control or ω3 PUFA-rich diet (adjusted to fat calorie 45%) for the indicated periods. *$p < 0.05$, control diet WT versus control diet KO; $^{\#}p < 0.05$, control diet WT versus ω3-rich diet WT; and $^{\$}p < 0.05$, control diet WT versus ω3-rich diet KO by ANOVA Dunnett's test.

(H) Quantitative RT-PCR of *Ucp1* in sWAT of WT and KO mice fed a control or ω3 PUFA-rich diet for 10 weeks. Mice were treated with CL316,243 (1 mg/kg body weight) or saline for 3 days.

(I) Quantitative RT-PCR of *Tnf* in vWAT of WT and KO mice fed a control or ω3 PUFA-rich diet for 10 weeks.

In (C)–(F), (H), and (I), expression levels of individual genes are normalized with *Gapdh*. Data are compiled from (A), (B), and (F)–(I) or representative of two experiments (C–E). In (B) and (G)–(I), sample sizes (n) are indicated in the figure. Mean ± SEM, *$p < 0.05$, **$p < 0.01$.

See also Figure S6.

was still high (Figure S3A), the levels of EPA and DHA, and to a lesser extent AA, were lower in the WAT (Figure S6A) and lymph nodes (Figure S6B) of *Pla2g2d*$^{-/-}$ mice than in those of *Pla2g2d*$^{+/+}$ mice. This fatty acid selectivity agrees with the enzymatic activity of PLA2G2D, which preferentially releases PUFAs, ω3 in particular (Miki et al., 2013). After HFD feeding for 20 weeks, when *Pla2g2d* expression was downregulated (Figure 1A), the decreased levels of PUFAs (EPA and DHA in particular, primarily due to their low content in HFD) were indistinguishable between the genotypes (Figure 5B). These results suggest that PLA2G2D constitutively supplies nearly half of the free PUFAs (preferentially ω3 EPA and DHA) in WAT under normal to an early stage

of HFD conditions, thereby delaying the ongoing process of diet-induced obesity. Phospholipid levels in WAT were barely altered by PLA2G2D deficiency, most likely because the local changes of phospholipids by $sPLA_2$s in a subset of cells were masked by high background levels of bulk phospholipids in the whole tissue.

However, the WAT levels of most ω3/ω6 PUFA-derived lipid mediators detected so far did not differ significantly between *Pla2g2d*$^{+/+}$ and *Pla2g2d*$^{-/-}$ mice (Figure S6C), suggesting that PLA2G2D-driven PUFAs in WAT are hardly converted to lipid mediators, the latter being produced mainly from a PLA2G2D-independent PUFA pool. In comparison, the WAT levels of PUFAs and their metabolites were not profoundly affected in mice lacking PLA2G5, a diet-inducible $sPLA_2$ that preferentially releases OA and LA from LDL phospholipids (Sato et al., 2014), or PLA2G4A (also known as $cPLA_2\alpha$) (Figures S6D and S6E), which is thought to be coupled with canonical AA metabolism in many tissues (Shimizu, 2009). Thus, generation of PUFA-derived lipid mediators in WAT may be mostly regulated by other phospholipases or lipases.

PUFAs by themselves have beneficial actions on metabolism, inflammation, and thermogenesis through several mechanisms involving GPR120, PPARγ, or others (Fan et al., 2019). Indeed, M1 polarization of BMDMs by palmitic acid, as monitored by induction of several M1 markers, was partially (for *Nos2* and *Il1b*) or almost entirely (for *Il6*) dampened by PUFAs including LA, AA, EPA, and DHA (Figure 5C). 9- and 13-hydroxyoctadecaenoic acids (HODEs), the most abundant lipid mediators detected in WAT thus far (Figure S6C), were ineffective (Figure 5C). The induction of *Nos2* was suppressed partially by either GSK137647 (GPR120 agonist) or pioglitazone (PPARγ agonist), that of *Il1b* was reduced partially by GSK137647 but not by pioglitazone, and that of *Il6* was almost totally insensitive to both agents (Figure 5C). Thus, PUFAs attenuate the expression of these pro-inflammatory M1 macrophage markers through multiple mechanisms. Furthermore, consistent with a recent study (Quesada-López et al., 2016), EPA and DHA as well as α-linolenic acid (ALA; C18:3 ω3), but not ω6 PUFAs (LA and AA), increased the expression of *Ucp1*, which was largely blunted by the GPR120 antagonist AH7614, in sWAT-derived, *ex-vivo*-differentiated primary adipocytes (Figures 5D and 5E), supporting the notion that ω3 PUFAs can promote adipocyte browning through acting on GPR120.

ω3 PUFA Supplementation Restores Metabolic Alterations in *Pla2g2d*$^{-/-}$ Mice

We next examined whether the metabolic alterations observed in *Pla2g2d*$^{-/-}$ mice could be restored by supplementation with ω3 PUFAs. To this end, sWAT was isolated from *Pla2g2d*$^{+/+}$ and *Pla2g2d*$^{-/-}$ mice and stimulated with CL316,243 in the presence or absence of EPA in an *ex vivo* culture. Consistent with the *in vivo* results (Figure 4E), the expression of *Ucp1* was significantly lower in the sWAT explant of *Pla2g2d*$^{-/-}$ mice than in that of *Pla2g2d*$^{+/+}$ mice (Figure 5F). Addition of EPA to the culture increased *Ucp1* expression in *Pla2g2d*$^{-/-}$ sWAT to a level similar to that in *Pla2g2d*$^{+/+}$ sWAT (Figure 5F), indicating that the decreased adipocyte browning in *Pla2g2d*$^{-/-}$ mice could be restored by exogenous EPA *ex vivo*. To further address this issue *in vivo*, *Pla2g2d*$^{+/+}$ and *Pla2g2d*$^{-/-}$ mice were fed an ω3 PUFA-rich diet in comparison with a lard-rich control diet, with 45% fat calorie in both diets. Consistent with Figure 2B, *Pla2g2d*$^{-/-}$ mice gained more weight than did *Pla2g2d*$^{+/+}$ mice under lard-rich diet conditions (Figure 5G). Strikingly, following ω3 PUFA-rich diet feeding, the weight gain tended to be milder in both *Pla2g2d*$^{+/+}$ and *Pla2g2d*$^{-/-}$ mice, with no difference between the genotypes at each time point (Figure 5G). When these mice were treated with CL316,243 at 10 weeks, *Ucp1* expression in sWAT was lower in *Pla2g2d*$^{-/-}$ mice than in *Pla2g2d*$^{+/+}$ mice on the lard-rich control diet, whereas feeding of the ω3 PUFA-rich diet increased *Ucp1* expression in sWAT of both *Pla2g2d*$^{+/+}$ and *Pla2g2d*$^{-/-}$ mice to a similar level (Figure 5H), as in the case of the *ex vivo* results (Figure 5F). Moreover, although vWAT expression of *Tnf* tended to be greater in *Pla2g2d*$^{-/-}$ mice than in *Pla2g2d*$^{+/+}$ mice after feeding of the lard-rich diet, this event was not evident in these mice after feeding of the ω3 PUFA-rich diet (Figure 5I). These results collectively suggest that the metabolic alterations in *Pla2g2d*$^{-/-}$ mice, including reduced adipocyte browning, increased diet-induced obesity, and increased WAT inflammation, are almost fully rescued by ω3 PUFA supplementation. Thus, we conclude that PLA2G2D constitutively supplies a pool of ω3 PUFAs in WAT, thereby contributing to maintenance of metabolic health by promoting adipocyte browning and by ameliorating chronic inflammation.

DISCUSSION

It has been well recognized that PUFAs, particularly ω3 PUFAs, have beneficial effects on systemic metabolism (Fan et al., 2019). Dietary treatment of experimental animals with ω3 PUFAs or fish oil (Itariu et al., 2012; Neuhofer et al., 2013) or transgenic overexpression of *fat-1*, which encodes an ω3 PUFA-producing desaturase in *Caenorhabditis elegans*, in mice (White et al., 2010) ameliorates obesity-associated inflammation and insulin resistance. ω3 PUFAs can also promote BAT recruitment and WAT browning in association with enhanced sympathetic neuronal tone, which eventually prevents obesity-related metabolic complications (Flachs et al., 2011; Kim et al., 2015, 2016; Laiglesia et al., 2016; Sadurskis et al., 1995; Villarroya et al., 2014; Zhao and Chen, 2014). Mechanistically, ω3 (and in some cases ω6) PUFAs exert their advantageous metabolic effects through their conversion to anti-inflammatory or pro-resolving lipid mediators (Clària et al., 2012; González-Périz et al., 2009; Neuhofer et al., 2013; Titos et al., 2011), their direct action on PUFA-sensing receptors (e.g., GPR120 and PPARs) (Cipolletta et al., 2012; Hamaguchi and Sakaguchi, 2012; Oishi et al., 2017), or attenuation of endoplasmic reticulum (ER) stress by increasing membrane fluidity after being incorporated into membrane phospholipids (Ariyama et al., 2010), among other mechanisms. Indeed, genetic deletion or mutation of GPR120, an ω3 PUFA receptor (Ichimura et al., 2012; Oh et al., 2010, 2014; Quesada-López et al., 2016; Yan et al., 2013), or LPCAT3, a lysophospholipid acyltransferase that preferentially incorporates PUFAs into membrane phospholipids (Rong et al., 2017; Wang et al., 2016), leads to metabolic perturbations.

Because a large proportion of PUFAs are stored in membrane phospholipids and spatiotemporally released by PLA_2 enzymes,

there has been increasing interest in the identity of a specific PLA_2(s) that supplies PUFAs in metabolically active tissues for metabolic regulation. In this study, we have provided evidence that PLA2G2D, a member of the $sPLA_2$ family, is responsible for this process. Recent studies using mice deficient in various $sPLA_2$ isoforms, which show different substrate specificities and tissue distributions, have revealed that these enzymes participate in various biological events, including exacerbation or prevention of inflammatory, metabolic, and other diseases, by driving distinct lipid pathways in given tissue microenvironments (Boudreau et al., 2014; Labonté et al., 2010; Miki et al., 2013; Murase et al., 2016; Sato et al., 2014; Taketomi et al., 2013; Yamamoto et al., 2015). Of these, PLA2G2D is expressed abundantly in lymphatic dendritic cells and macrophages, putting a brake on harmful immune responses in Th1-driven contact dermatitis and Th17-driven psoriasis by constitutively supplying ω3 PUFA-derived pro-resolving lipid mediators (Miki et al., 2013, 2016). Here we have shown that PLA2G2D is preferentially and constitutively expressed in M2-like macrophages within WAT and exhibits a reciprocal correlation with obesity and insulin resistance. This expression profile of PLA2G2D contrasts with that of PLA2G5 and PLA2G2E, which are induced in hypertrophic adipocytes during obesity (Sato et al., 2014). Downregulation of *Pla2g2d* during inflammation, such as in LPS-stimulated macrophages and in antigen-captured major histocompatibility complex (MHC) class II^{hi} dendritic cells, has also been demonstrated in previous studies (Miki et al., 2013, 2016; von Allmen et al., 2009). Considering that obesity is accompanied by chronic inflammation in WAT, with a myriad of pro-inflammatory factors in adipose tissue microenvironments, it is plausible that *Pla2g2d* expression declines with obesity in response to one or more of these pro-inflammatory factors. Indeed, our data show that palmitic acid, a pro-inflammatory SFA that is abundantly present in adipose tissue during obesity, reduces *Pla2g2d* expression in macrophages.

Importantly, both global and macrophage-specific deletions of PLA2G2D lead to exacerbation of diet-induced obesity, insulin resistance, and adipose tissue inflammation, a finding that supports the anti-inflammatory role of this enzyme as a "resolving $sPLA_2$" (Miki et al., 2013). Because the absence of PLA2G2D does not profoundly affect the liver and BAT, where the expression of this enzyme is very low, it is likely that PLA2G2D expressed locally in WAT plays a leading role in metabolic regulation. However, considering an increased expression of Th1 cytokines and a marked reduction of anti-inflammatory ω3 PUFAs in regional lymph nodes of *Pla2g2d*$^{-/-}$ mice at an early stage of diet-induced obesity, it is possible that an anti-inflammatory state in lymph organs mediated by PLA2G2D-driven ω3 PUFA metabolites (Miki et al., 2013) might also contribute, at least partly, to the anti-obesity function of this enzyme. Indeed, lymph node cells in *Pla2g2d*$^{-/-}$ mice are prone to be hyperactivated in the contexts of Th1-driven contact hypersensitivity and Th17-driven psoriasis (Miki et al., 2013, 2016), suggesting that *Pla2g2d* deficiency promotes M1 skewing of macrophages at the onset of disease.

Understanding the molecular mechanisms and signaling networks that induce beige adipocytes is of fundamental importance for research aimed at obesity prevention (Harms and Seale, 2013; Kajimura et al., 2015). Reductions in beige fat activity predispose animals to the harmful metabolic effects of an HFD (Cohen et al., 2014). Beyond a recent study using transgenic mice overexpressing PLA2G2A ($sPLA_2$-IIA), in which WAT was shown to be more prone to adipocyte browning with increased expression of thermogenic markers (Kuefner et al., 2019), the present study highlights that an endogenous $sPLA_2$, i.e., PLA2G2D, does regulate adipocyte browning and adaptive thermogenesis. This function of PLA2G2D is consistent with its more abundant expression in sWAT, the primary site for cold-induced adipocyte browning, than in vWAT. It has been well documented that various types of immune cells residing in WAT closely interact with adipocytes and regulate metabolic homeostasis in positive and negative ways (Brestoff and Artis, 2015). In particular, type 2 immunity involving type 2 innate lymphoid cells (ILC2s), eosinophils, and M2 macrophages exerts accelerating effects on adipocyte browning (Nguyen et al., 2011; Qiu et al., 2014; Rao et al., 2014; Wu et al., 2011). Although M2 macrophages were initially proposed to promote adipocyte browning by synthesizing norepinephrine (Nguyen et al., 2011), this idea has recently been challenged by others (Fischer et al., 2017; Jiang et al., 2017). Rather, a population of adipose tissue macrophages influences β_3-adrenergic tone by taking up and degrading, rather than synthesizing, norepinephrine (Camell et al., 2017; Pirzgalska et al., 2017) or by inhibiting sympathetic innervation over time (Wolf et al., 2017). Regardless of the norepinephrine paradox, other studies have recently shown that some natural ligands for PPARγ, a nuclear receptor that binds to ω3 PUFAs (Lee et al., 2013, 2016), and acetylcholine, which acts on the nicotinic receptor CHRNA2 (Jun et al., 2018), serve as M2 macrophage-derived paracrine factors that facilitate adipocyte browning. Our present study appears to fit with the former notion, underscoring PLA2G2D as a previously unrecognized factor that links M2-like macrophages to adipocyte browning through the supply of PUFAs.

Pla2g2d deficiency leads to significant reduction of PUFAs, particularly ω3 EPA and DHA, without alterations to their oxygenated metabolites in WAT, suggesting that the metabolic regulation by PLA2G2D relies largely, even if not solely, on the supply of a pool of PUFAs themselves. Among a number of local factors that can affect adipocyte browning (Reitman, 2017; Villarroya et al., 2018), FGF21 produced by adipocytes in response to β_3-adrenergic signals integrates type 2 immunity and adipocyte browning (Huang et al., 2017). ω3 PUFAs, by acting on the PUFA receptor GPR120 (Quesada-López et al., 2016) or PPARγ (Qiang et al., 2012; Vernochet et al., 2009; Wang et al., 2016), augment FGF21 production by adipocytes and thereby facilitate adipocyte browning and thermogenesis. Consistently, we have shown here that ω3 (rather than ω6) PUFAs are capable of upregulating *Ucp1* expression in sWAT-derived adipocytes in a manner dependent upon GPR120. Indeed, the exacerbated metabolic phenotypes observed in *Pla2g2d*$^{-/-}$ mice are similar in many aspects to those observed in mice lacking GPR120 (*Ffar4*$^{-/-}$), which also display increased diet-induced obesity, insulin resistance, and adipose tissue inflammation, in association with reduced energy expenditure, adipocyte browning, thermogenesis, and FGF21 expression (Ichimura et al., 2012; Oh et al., 2010, 2014; Quesada-

López et al., 2016; Yan et al., 2013). Thus, the functional interaction between M2-type macrophages and beige adipocytes through the PLA2G2D-ω3 PUFA-GPR120 axis may coordinate organismal fitness after environmental challenges to cold, whereas perturbation of this regulatory pathway hampers metabolic homeostasis upon nutritional overload. From this standpoint, the M1-skewed inflammatory profile in WAT of HFD-fed *Pla2g2d*$^{-/-}$ mice might be a consequence, rather than a cause, of the increased obesity resulting from reduced adipocyte browning and thereby energy expenditure, although the possibility that the decreased anti-inflammatory ω3 PUFA tone might additionally affect the property of macrophages cannot be fully ruled out. In support of the latter idea, macrophages in lymphoid organs are skewed into M1-like macrophages in *Pla2g2d*$^{-/-}$ mice even under normal conditions, most likely due to the reduction of ω3 PUFAs (Miki et al., 2016).

Because sPLA$_2$ hydrolyzes phospholipids in extracellular microparticles or exosomes (Boudreau et al., 2014) and adipose tissue is a rich source of such extracellular vesicles (Crewe et al., 2018; Thomou et al., 2017), it is tempting to speculate that PLA2G2D secreted from M2-type macrophages within a WAT niche may hydrolyze phospholipids in adipocyte-derived extracellular vesicles to release a pool of free PUFAs that are not readily accessible to downstream enzymes for lipid mediator biosynthesis. Alternatively, because M2-type macrophages can support adipocyte browning through elimination of cell remnants in association with PPARγ ligand synthesis during tissue remodeling (Lee et al., 2016), PLA2G2D may release PUFAs from the remnant membranes. Such a PUFA pool spatiotemporally mobilized by PLA2G2D in WAT may in turn promote adipocyte browning through GPR120- and/or PPARγ-dependent processes or through alternative mechanisms such as attenuation of ER stress (Okla et al., 2015). It is also possible that certain PUFA-derived metabolites that were not evaluated in this study might also be involved in PLA2G2D action.

It is noteworthy that >50% of free PUFAs still remained in *Pla2g2d*$^{-/-}$ WAT, suggesting the existence of a different route(s) for the supply of PUFAs that could be coupled with their conversion to lipid mediators. Our results using *Pla2g4a*$^{-/-}$ mice suggest that the contribution of PLA2G4A (cPLA$_2$α), a canonical regulator of AA metabolism (Shimizu, 2009), to eicosanoid synthesis is negligible in WAT, arguing for the role of other PLA$_2$s. It has been reported that PLA2G16 (adipose-specific PLA) is linked to PGE$_2$ generation in WAT (Jaworski et al., 2009), although subsequent studies have claimed that this enzyme has more robust PLA$_1$ than PLA$_2$ activity and might participate in lipid metabolism other than eicosanoid generation (Pang et al., 2012; Uyama et al., 2012). Alternatively, the PUFA-derived mediators in WAT may be supplied from neutral lipids through the lipolytic pathway involving adipose triglyceride lipase (ATGL; also known as PNPLA2 or iPLA$_2$ζ), hormone-sensitive lipase, and monoacylglycerol lipase. Indeed, pharmacological or genetic inactivation of these lipases alleviates the generation of AA metabolites in several situations (Dichlberger et al., 2014; Nomura et al., 2011; Ogasawara et al., 2016), and EPA-derived 12-hydroxyeicosapentaenoic acid (12-HEPE), which is produced by the sequential action of ATGL and 12-lipoxygenase, regulates BAT functions (Leiria et al., 2019).

In conclusion, the present study has highlighted PLA2G2D as a regulator of metabolic health. The PLA2G2D-ω3 PUFA axis facilitates energy expenditure through increased adipocyte browning and thermogenesis, thereby protecting against diet-induced obesity, adipose tissue inflammation, and insulin resistance. Thus, when considered along with the results of our previous study (Sato et al., 2014), it appears that three sPLA$_2$s (PLA2G2D, PLA2G2E, and PLA2G5) spatiotemporally expressed in distinct cells within WAT exert different impacts on systemic metabolism through mobilization of distinct lipid pathways (Figure 6). From the standpoint of PLA$_2$ biology, PLA2G2D acts not merely as a "resolving sPLA$_2$" that sequesters inflammation (Miki et al., 2013) but also as a "thermogenic sPLA$_2$" that facilitates adaptive thermogenesis, a property that is not shared by other sPLA$_2$s or any other PLA$_2$ subtypes reported so far. Because PLA2G2D is also expressed in human macrophages and its potential role in human body weight control has been suggested from a study employing a SNP in the *PLA2G2D* gene (Takabatake et al., 2005), it is likely that the enzyme may also play similar roles in humans. Our results point to potential prophylactic or therapeutic use of PLA2G2D itself or an agent that could specifically stabilize or upregulate PLA2G2D to afford protection against metabolic diseases.

STAR★METHODS

Detailed methods are provided in the online version of this paper and include the following:

- KEY RESOURCES TABLE
- LEAD CONTACT AND MATERIALS AVAILABILITY
- EXPERIMENTAL MODEL AND SUBJECT DETAILS
  - Mice
  - Culture of BMDMs
  - Culture of primary adipocytes
  - *Ex vivo* culture of WAT explants
- METHOD DETAILS
  - Quantitative RT-PCR
  - Experiments using special diets
  - Adipocyte browning
  - Glucose and insulin tolerance tests
  - Oxygen consumption and locomotor activity
  - Immunoblotting
  - CT analysis
  - Histology and immunohistochemistry
  - Whole mount immunofluorescence microscopy of adipose tissue
  - Isolation of SVF
  - Flow cytometry
  - Measurement of serum markers
  - Lipidomics analysis
- QUANTIFICATION AND STATISTICAL ANALYSIS
- DATA AND CODE AVAILABILITY

SUPPLEMENTAL INFORMATION

Supplemental Information can be found online at https://doi.org/10.1016/j.celrep.2020.107579.

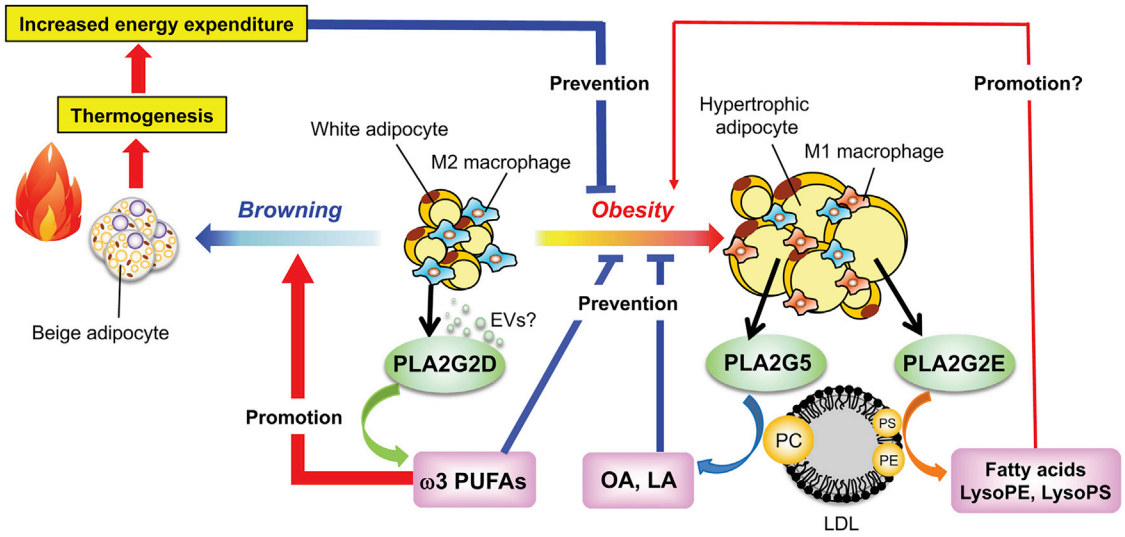

Figure 6. Schematic Diagram of Metabolic Regulation by sPLA$_2$s in WAT

In WAT, PLA2G5 and PLA2G2E are induced in hypertrophic adipocytes during obesity, whereas PLA2G2D is constitutively expressed in M2-type macrophages in lean WAT. Obesity-induced PLA2G5 prevents metabolic disorders by hydrolyzing PC in low-density lipoprotein (LDL) to supply OA and LA, which attenuate palmitate-induced M1 macrophage skewing, whereas PLA2G2E hydrolyzes minor lipoprotein phospholipids (PE and PS) and increases adiposity through an unknown mechanism (Sato et al., 2014). PLA2G2D, which preferentially releases ω3 PUFAs possibly from phospholipids in extracellular vesicles (EVs), promotes adipocyte browning and thermogenesis, thereby counteracting obesity-associated metabolic complications and WAT inflammation.

ACKNOWLEDGMENTS

We thank Dr. Michal H. Gelb (University of Washington) for kindly providing us global and conditional *Pla2g2d*-deficient mice. This work was supported by JSPS KAKENHI grants JP15H05905, JP16H02613, and JP18H05025 (to M.M.), JP25860059, JP15K07959, and JP18K06128 (to H.S.), JP18K06624 (to Y.T.), and JP16K18882 (to Y.M.); and AMED-CREST JP18gm0710006 and AMED-FORCE 19gm4010005 (to M.M.) from the Japan Agency for Medical Research and Development, the Kowa Life Science Foundation, the Ono Medical Research Foundation, and the Astellas Foundation for Research on Metabolic Disorders (to H.S.).

AUTHOR CONTRIBUTIONS

M.M. and H.S. designed the study and wrote the manuscript, and Y.T., Y.M., R.M., and K.Y. performed several parts of the experiments and data analysis.

DECLARATION OF INTERESTS

The authors declare no competing interests.

Received: January 4, 2019
Revised: November 18, 2019
Accepted: April 7, 2020
Published: May 5, 2020

REFERENCES

Ariyama, H., Kono, N., Matsuda, S., Inoue, T., and Arai, H. (2010). Decrease in membrane phospholipid unsaturation induces unfolded protein response. J. Biol. Chem. *285*, 22027–22035.

Boström, P., Wu, J., Jedrychowski, M.P., Korde, A., Ye, L., Lo, J.C., Rasbach, K.A., Boström, E.A., Choi, J.H., Long, J.Z., et al. (2012). A PGC1-α-dependent myokine that drives brown-fat-like development of white fat and thermogenesis. Nature *481*, 463–468.

Boudreau, L.H., Duchez, A.C., Cloutier, N., Soulet, D., Martin, N., Bollinger, J., Paré, A., Rousseau, M., Naika, G.S., Lévesque, T., et al. (2014). Platelets release mitochondria serving as substrate for bactericidal group IIA-secreted phospholipase A$_2$ to promote inflammation. Blood *124*, 2173–2183.

Brestoff, J.R., and Artis, D. (2015). Immune regulation of metabolic homeostasis in health and disease. Cell *161*, 146–160.

Camell, C.D., Sander, J., Spadaro, O., Lee, A., Nguyen, K.Y., Wing, A., Goldberg, E.L., Youm, Y.H., Brown, C.W., Elsworth, J., et al. (2017). Inflammasome-driven catecholamine catabolism in macrophages blunts lipolysis during ageing. Nature *550*, 119–123.

Cao, H., Gerhold, K., Mayers, J.R., Wiest, M.M., Watkins, S.M., and Hotamisligil, G.S. (2008). Identification of a lipokine, a lipid hormone linking adipose tissue to systemic metabolism. Cell *134*, 933–944.

Cao, L., Choi, E.Y., Liu, X., Martin, A., Wang, C., Xu, X., and During, M.J. (2011). White to brown fat phenotypic switch induced by genetic and environmental activation of a hypothalamic-adipocyte axis. Cell Metab. *14*, 324–338.

Cipolletta, D., Feuerer, M., Li, A., Kamei, N., Lee, J., Shoelson, S.E., Benoist, C., and Mathis, D. (2012). PPAR-γ is a major driver of the accumulation and phenotype of adipose tissue Treg cells. Nature *486*, 549–553.

Clària, J., Dalli, J., Yacoubian, S., Gao, F., and Serhan, C.N. (2012). Resolvin D1 and resolvin D2 govern local inflammatory tone in obese fat. J. Immunol. *189*, 2597–2605.

Cohen, P., Levy, J.D., Zhang, Y., Frontini, A., Kolodin, D.P., Svensson, K.J., Lo, J.C., Zeng, X., Ye, L., Khandekar, M.J., et al. (2014). Ablation of PRDM16 and beige adipose causes metabolic dysfunction and a subcutaneous to visceral fat switch. Cell *156*, 304–316.

Crewe, C., Joffin, N., Rutkowski, J.M., Kim, M., Zhang, F., Towler, D.A., Gordillo, R., and Scherer, P.E. (2018). An endothelial-to-adipocyte extracellular vesicle axis governed by metabolic state. Cell *175*, 695–708.e13.

Dichlberger, A., Schlager, S., Maaninka, K., Schneider, W.J., and Kovanen, P.T. (2014). Adipose triglyceride lipase regulates eicosanoid production in activated human mast cells. J. Lipid Res. *55*, 2471–2478.

Fan, R., Koehler, K., and Chung, S. (2019). Adaptive thermogenesis by dietary n-3 polyunsaturated fatty acids: emerging evidence and mechanisms. Biochim. Biophys. Acta Mol. Cell Biol. Lipids *1864*, 59–70.

Fischer, K., Ruiz, H.H., Jhun, K., Finan, B., Oberlin, D.J., van der Heide, V., Kalinovich, A.V., Petrovic, N., Wolf, Y., Clemmensen, C., et al. (2017). Alternatively activated macrophages do not synthesize catecholamines or contribute to adipose tissue adaptive thermogenesis. Nat. Med. *23*, 623–630.

Fisher, F.M., Kleiner, S., Douris, N., Fox, E.C., Mepani, R.J., Verdeguer, F., Wu, J., Kharitonenkov, A., Flier, J.S., Maratos-Flier, E., and Spiegelman, B.M. (2012). FGF21 regulates PGC-1α and browning of white adipose tissues in adaptive thermogenesis. Genes Dev. *26*, 271–281.

Flachs, P., Rühl, R., Hensler, M., Janovska, P., Zouhar, P., Kus, V., Macek Jilkova, Z., Papp, E., Kuda, O., Svobodova, M., et al. (2011). Synergistic induction of lipid catabolism and anti-inflammatory lipids in white fat of dietary obese mice in response to calorie restriction and n-3 fatty acids. Diabetologia *54*, 2626–2638.

González-Périz, A., Horrillo, R., Ferré, N., Gronert, K., Dong, B., Morán-Salvador, E., Titos, E., Martínez-Clemente, M., López-Parra, M., Arroyo, V., and Clària, J. (2009). Obesity-induced insulin resistance and hepatic steatosis are alleviated by ω-3 fatty acids: a role for resolvins and protectins. FASEB J. *23*, 1946–1957.

Haemmerle, G., Lass, A., Zimmermann, R., Gorkiewicz, G., Meyer, C., Rozman, J., Heldmaier, G., Maier, R., Theussl, C., Eder, S., et al. (2006). Defective lipolysis and altered energy metabolism in mice lacking adipose triglyceride lipase. Science *312*, 734–737.

Hamaguchi, M., and Sakaguchi, S. (2012). Regulatory T cells expressing PPAR-γ control inflammation in obesity. Cell Metab. *16*, 4–6.

Hanssen, M.J., Hoeks, J., Brans, B., van der Lans, A.A., Schaart, G., van den Driessche, J.J., Jörgensen, J.A., Boekschoten, M.V., Hesselink, M.K., Havekes, B., et al. (2015). Short-term cold acclimation improves insulin sensitivity in patients with type 2 diabetes mellitus. Nat. Med. *21*, 863–865.

Harms, M., and Seale, P. (2013). Brown and beige fat: development, function and therapeutic potential. Nat. Med. *19*, 1252–1263.

Harms, M.J., Ishibashi, J., Wang, W., Lim, H.W., Goyama, S., Sato, T., Kurokawa, M., Won, K.J., and Seale, P. (2014). Prdm16 is required for the maintenance of brown adipocyte identity and function in adult mice. Cell Metab. *19*, 593–604.

Holzer, R.G., Park, E.J., Li, N., Tran, H., Chen, M., Choi, C., Solinas, G., and Karin, M. (2011). Saturated fatty acids induce c-Src clustering within membrane subdomains, leading to JNK activation. Cell *147*, 173–184.

Huang, Z., Zhong, L., Lee, J.T.H., Zhang, J., Wu, D., Geng, L., Wang, Y., Wong, C.M., and Xu, A. (2017). The FGF21-CCL11 axis mediates beiging of white adipose tissues by coupling sympathetic nervous system to type 2 immunity. Cell Metab. *26*, 493–508.e4.

Hui, X., Gu, P., Zhang, J., Nie, T., Pan, Y., Wu, D., Feng, T., Zhong, C., Wang, Y., Lam, K.S., and Xu, A. (2015). Adiponectin enhances cold-induced browning of subcutaneous adipose tissue via promoting M2 macrophage proliferation. Cell Metab. *22*, 279–290.

Ichimura, A., Hirasawa, A., Poulain-Godefroy, O., Bonnefond, A., Hara, T., Yengo, L., Kimura, I., Leloire, A., Liu, N., Iida, K., et al. (2012). Dysfunction of lipid sensor GPR120 leads to obesity in both mouse and human. Nature *483*, 350–354.

Itariu, B.K., Zeyda, M., Hochbrugger, E.E., Neuhofer, A., Prager, G., Schindler, K., Bohdjalian, A., Mascher, D., Vangala, S., Schranz, M., et al. (2012). Long-chain n-3 PUFAs reduce adipose tissue and systemic inflammation in severely obese nondiabetic patients: a randomized controlled trial. Am. J. Clin. Nutr. *96*, 1137–1149.

Jaworski, K., Ahmadian, M., Duncan, R.E., Sarkadi-Nagy, E., Varady, K.A., Hellerstein, M.K., Lee, H.Y., Samuel, V.T., Shulman, G.I., Kim, K.H., et al. (2009). AdPLA ablation increases lipolysis and prevents obesity induced by high-fat feeding or leptin deficiency. Nat. Med. *15*, 159–168.

Jiang, H., Ding, X., Cao, Y., Wang, H., and Zeng, W. (2017). Dense intra-adipose sympathetic arborizations are essential for cold-induced beiging of mouse white adipose tissue. Cell Metab. *26*, 686–692.e3.

Jun, H., Yu, H., Gong, J., Jiang, J., Qiao, X., Perkey, E., Kim, D.I., Emont, M.P., Zestos, A.G., Cho, J.S., et al. (2018). An immune-beige adipocyte communication via nicotinic acetylcholine receptor signaling. Nat. Med. *24*, 814–822.

Kadl, A., Meher, A.K., Sharma, P.R., Lee, M.Y., Doran, A.C., Johnstone, S.R., Elliott, M.R., Gruber, F., Han, J., Chen, W., et al. (2010). Identification of a novel macrophage phenotype that develops in response to atherogenic phospholipids via Nrf2. Circ. Res. *107*, 737–746.

Kajimura, S., Spiegelman, B.M., and Seale, P. (2015). Brown and beige fat: physiological roles beyond heat generation. Cell Metab. *22*, 546–559.

Kim, M., Goto, T., Yu, R., Uchida, K., Tominaga, M., Kano, Y., Takahashi, N., and Kawada, T. (2015). Fish oil intake induces UCP1 upregulation in brown and white adipose tissue via the sympathetic nervous system. Sci. Rep. *5*, 18013.

Kim, J., Okla, M., Erickson, A., Carr, T., Natarajan, S.K., and Chung, S. (2016). Eicosapentaenoic acid potentiates brown thermogenesis through FFAR4-dependent up-regulation of miR-30b and miR-378. J. Biol. Chem. *291*, 20551–20562.

Kim, M., Furuzono, T., Yamakuni, K., Li, Y., Kim, Y.I., Takahashi, H., Ohue-Kitano, R., Jheng, H.F., Takahashi, N., Kano, Y., et al. (2017). 10-oxo-12(*Z*)-octadecenoic acid, a linoleic acid metabolite produced by gut lactic acid bacteria, enhances energy metabolism by activation of TRPV1. FASEB J. *31*, 5036–5048.

Kozak, L.P. (2010). Brown fat and the myth of diet-induced thermogenesis. Cell Metab. *11*, 263–267.

Kuefner, M.S., Deng, X., Stephenson, E.J., Pham, K., and Park, E.A. (2019). Secretory phospholipase A_2 group IIA enhances the metabolic rate and increases glucose utilization in response to thyroid hormone. FASEB J. *33*, 738–749.

Labonté, E.D., Pfluger, P.T., Cash, J.G., Kuhel, D.G., Roja, J.C., Magness, D.P., Jandacek, R.J., Tschöp, M.H., and Hui, D.Y. (2010). Postprandial lysophospholipid suppresses hepatic fatty acid oxidation: the molecular link between group 1B phospholipase A_2 and diet-induced obesity. FASEB J. *24*, 2516–2524.

Laiglesia, L.M., Lorente-Cebrián, S., Prieto-Hontoria, P.L., Fernández-Galilea, M., Ribeiro, S.M., Sáinz, N., Martínez, J.A., and Moreno-Aliaga, M.J. (2016). Eicosapentaenoic acid promotes mitochondrial biogenesis and beige-like features in subcutaneous adipocytes from overweight subjects. J. Nutr. Biochem. *37*, 76–82.

Lee, Y.H., Petkova, A.P., and Granneman, J.G. (2013). Identification of an adipogenic niche for adipose tissue remodeling and restoration. Cell Metab. *18*, 355–367.

Lee, P., Linderman, J.D., Smith, S., Brychta, R.J., Wang, J., Idelson, C., Perron, R.M., Werner, C.D., Phan, G.Q., Kammula, U.S., et al. (2014). Irisin and FGF21 are cold-induced endocrine activators of brown fat function in humans. Cell Metab. *19*, 302–309.

Lee, M.W., Odegaard, J.I., Mukundan, L., Qiu, Y., Molofsky, A.B., Nussbaum, J.C., Yun, K., Locksley, R.M., and Chawla, A. (2015). Activated type 2 innate lymphoid cells regulate beige fat biogenesis. Cell *160*, 74–87.

Lee, Y.H., Kim, S.N., Kwon, H.J., Maddipati, K.R., and Granneman, J.G. (2016). Adipogenic role of alternatively activated macrophages in β-adrenergic remodeling of white adipose tissue. Am. J. Physiol. Regul. Integr. Comp. Physiol. *310*, R55–R65.

Leiria, L.O., Wang, C.H., Lynes, M.D., Yang, K., Shamsi, F., Sato, M., Sugimoto, S., Chen, E.Y., Bussberg, V., Narain, N.R., et al. (2019). 12-lipoxygenase regulates cold adaptation and glucose metabolism by producing the omega-3 lipid 12-HEPE from brown fat. Cell Metab. *30*, 768–783.e7.

Li, P., Oh, D.Y., Bandyopadhyay, G., Lagakos, W.S., Talukdar, S., Osborn, O., Johnson, A., Chung, H., Maris, M., Ofrecio, J.M., et al. (2015). LTB_4 promotes insulin resistance in obese mice by acting on macrophages, hepatocytes and myocytes. Nat. Med. *21*, 239–247.

Long, J.Z., Svensson, K.J., Bateman, L.A., Lin, H., Kamenecka, T., Lokurkar, I.A., Lou, J., Rao, R.R., Chang, M.R., Jedrychowski, M.P., et al. (2016). The secreted enzyme PM20D1 regulates lipidated amino acid uncouplers of mitochondria. Cell *166*, 424–435.

Lynes, M.D., Leiria, L.O., Lundh, M., Bartelt, A., Shamsi, F., Huang, T.L., Takahashi, H., Hirshman, M.F., Schlein, C., Lee, A., et al. (2017). The cold-induced lipokine 12,13-diHOME promotes fatty acid transport into brown adipose tissue. Nat. Med. *23*, 631–637.

Mancuso, D.J., Sims, H.F., Yang, K., Kiebish, M.A., Su, X., Jenkins, C.M., Guan, S., Moon, S.H., Pietka, T., Nassir, F., et al. (2010). Genetic ablation of calcium-independent phospholipase $A_2\gamma$ prevents obesity and insulin resistance during high fat feeding by mitochondrial uncoupling and increased adipocyte fatty acid oxidation. J. Biol. Chem. *285*, 36495–36510.

Miki, Y., Yamamoto, K., Taketomi, Y., Sato, H., Shimo, K., Kobayashi, T., Ishikawa, Y., Ishii, T., Nakanishi, H., Ikeda, K., et al. (2013). Lymphoid tissue phospholipase A_2 group IID resolves contact hypersensitivity by driving antiinflammatory lipid mediators. J. Exp. Med. *210*, 1217–1234.

Miki, Y., Kidoguchi, Y., Sato, M., Taketomi, Y., Taya, C., Muramatsu, K., Gelb, M.H., Yamamoto, K., and Murakami, M. (2016). Dual roles of group IID phospholipase A_2 in inflammation and cancer. J. Biol. Chem. *291*, 15588–15601.

Murakami, M. (2017). Lipoquality control by phospholipase A_2 enzymes. Proc. Jpn. Acad. Ser. B Phys. Biol. Sci. *93*, 677–702.

Murase, R., Sato, H., Yamamoto, K., Ushida, A., Nishito, Y., Ikeda, K., Kobayashi, T., Yamamoto, T., Taketomi, Y., and Murakami, M. (2016). Group X secreted phospholipase A_2 releases ω3 polyunsaturated fatty acids, suppresses colitis, and promotes sperm fertility. J. Biol. Chem. *291*, 6895–6911.

Nedergaard, J., and Cannon, B. (2014). The browning of white adipose tissue: some burning issues. Cell Metab. *20*, 396–407.

Neuhofer, A., Zeyda, M., Mascher, D., Itariu, B.K., Murano, I., Leitner, L., Hochbrugger, E.E., Fraisl, P., Cinti, S., Serhan, C.N., and Stulnig, T.M. (2013). Impaired local production of proresolving lipid mediators in obesity and 17-HDHA as a potential treatment for obesity-associated inflammation. Diabetes *62*, 1945–1956.

Nguyen, K.D., Qiu, Y., Cui, X., Goh, Y.P., Mwangi, J., David, T., Mukundan, L., Brombacher, F., Locksley, R.M., and Chawla, A. (2011). Alternatively activated macrophages produce catecholamines to sustain adaptive thermogenesis. Nature *480*, 104–108.

Nomura, D.K., Morrison, B.E., Blankman, J.L., Long, J.Z., Kinsey, S.G., Marcondes, M.C., Ward, A.M., Hahn, Y.K., Lichtman, A.H., Conti, B., and Cravatt, B.F. (2011). Endocannabinoid hydrolysis generates brain prostaglandins that promote neuroinflammation. Science *334*, 809–813.

Ogasawara, D., Deng, H., Viader, A., Baggelaar, M.P., Breman, A., den Dulk, H., van den Nieuwendijk, A.M., Soethoudt, M., van der Wel, T., Zhou, J., et al. (2016). Rapid and profound rewiring of brain lipid signaling networks by acute diacylglycerol lipase inhibition. Proc. Natl. Acad. Sci. USA *113*, 26–33.

Oh, D.Y., Talukdar, S., Bae, E.J., Imamura, T., Morinaga, H., Fan, W., Li, P., Lu, W.J., Watkins, S.M., and Olefsky, J.M. (2010). GPR120 is an omega-3 fatty acid receptor mediating potent anti-inflammatory and insulin-sensitizing effects. Cell *142*, 687–698.

Oh, D.Y., Walenta, E., Akiyama, T.E., Lagakos, W.S., Lackey, D., Pessentheiner, A.R., Sasik, R., Hah, N., Chi, T.J., Cox, J.M., et al. (2014). A Gpr120-selective agonist improves insulin resistance and chronic inflammation in obese mice. Nat. Med. *20*, 942–947.

Ohno, H., Shinoda, K., Spiegelman, B.M., and Kajimura, S. (2012). PPARγ agonists induce a white-to-brown fat conversion through stabilization of PRDM16 protein. Cell Metab. *15*, 395–404.

Oishi, Y., Spann, N.J., Link, V.M., Muse, E.D., Strid, T., Edillor, C., Kolar, M.J., Matsuzaka, T., Hayakawa, S., Tao, J., et al. (2017). SREBP1 contributes to resolution of pro-inflammatory TLR4 signaling by reprogramming fatty acid metabolism. Cell Metab. *25*, 412–427.

Okla, M., Wang, W., Kang, I., Pashaj, A., Carr, T., and Chung, S. (2015). Activation of Toll-like receptor 4 (TLR4) attenuates adaptive thermogenesis via endoplasmic reticulum stress. J. Biol. Chem. *290*, 26476–26490.

Olefsky, J.M., and Glass, C.K. (2010). Macrophages, inflammation, and insulin resistance. Annu. Rev. Physiol. *72*, 219–246.

Pang, X.Y., Cao, J., Addington, L., Lovell, S., Battaile, K.P., Zhang, N., Rao, J.L., Dennis, E.A., and Moise, A.R. (2012). Structure/function relationships of adipose phospholipase A_2 containing a Cys-His-His catalytic triad. J. Biol. Chem. *287*, 35260–35274.

Peña, L., Meana, C., Astudillo, A.M., Lordén, G., Valdearcos, M., Sato, H., Murakami, M., Balsinde, J., and Balboa, M.A. (2016). Critical role for cytosolic group IVA phospholipase A_2 in early adipocyte differentiation and obesity. Biochim. Biophys. Acta *1861* (*9 Pt A*), 1083–1095.

Pirzgalska, R.M., Seixas, E., Seidman, J.S., Link, V.M., Sánchez, N.M., Mahú, I., Mendes, R., Gres, V., Kubasova, N., Morris, I., et al. (2017). Sympathetic neuron-associated macrophages contribute to obesity by importing and metabolizing norepinephrine. Nat. Med. *23*, 1309–1318.

Qiang, L., Wang, L., Kon, N., Zhao, W., Lee, S., Zhang, Y., Rosenbaum, M., Zhao, Y., Gu, W., Farmer, S.R., and Accili, D. (2012). Brown remodeling of white adipose tissue by SirT1-dependent deacetylation of Pparγ. Cell *150*, 620–632.

Qiu, Y., Nguyen, K.D., Odegaard, J.I., Cui, X., Tian, X., Locksley, R.M., Palmiter, R.D., and Chawla, A. (2014). Eosinophils and type 2 cytokine signaling in macrophages orchestrate development of functional beige fat. Cell *157*, 1292–1308.

Quesada-López, T., Cereijo, R., Turatsinze, J.V., Planavila, A., Cairó, M., Gavaldà-Navarro, A., Peyrou, M., Moure, R., Iglesias, R., Giralt, M., et al. (2016). The lipid sensor GPR120 promotes brown fat activation and FGF21 release from adipocytes. Nat. Commun. *7*, 13479.

Rao, R.R., Long, J.Z., White, J.P., Svensson, K.J., Lou, J., Lokurkar, I., Jedrychowski, M.P., Ruas, J.L., Wrann, C.D., Lo, J.C., et al. (2014). Meteorin-like is a hormone that regulates immune-adipose interactions to increase beige fat thermogenesis. Cell *157*, 1279–1291.

Reitman, M.L. (2017). How does fat transition from white to beige? Cell Metab. *26*, 14–16.

Roberts, L.D., Boström, P., O'Sullivan, J.F., Schinzel, R.T., Lewis, G.D., Dejam, A., Lee, Y.K., Palma, M.J., Calhoun, S., Georgiadi, A., et al. (2014). β-aminoisobutyric acid induces browning of white fat and hepatic β-oxidation and is inversely correlated with cardiometabolic risk factors. Cell Metab. *19*, 96–108.

Rong, X., Wang, B., Palladino, E.N., de Aguiar Vallim, T.Q., Ford, D.A., and Tontonoz, P. (2017). ER phospholipid composition modulates lipogenesis during feeding and in obesity. J. Clin. Invest. *127*, 3640–3651.

Rosenwald, M., Perdikari, A., Rülicke, T., and Wolfrum, C. (2013). Bi-directional interconversion of brite and white adipocytes. Nat. Cell Biol. *15*, 659–667.

Sadurskis, A., Dicker, A., Cannon, B., and Nedergaard, J. (1995). Polyunsaturated fatty acids recruit brown adipose tissue: increased UCP content and NST capacity. Am. J. Physiol. *269*, E351–E360.

Sato, H., Taketomi, Y., Ushida, A., Isogai, Y., Kojima, T., Hirabayashi, T., Miki, Y., Yamamoto, K., Nishito, Y., Kobayashi, T., et al. (2014). The adipocyte-inducible secreted phospholipases PLA2G5 and PLA2G2E play distinct roles in obesity. Cell Metab. *20*, 119–132.

Serhan, C.N. (2014). Pro-resolving lipid mediators are leads for resolution physiology. Nature *510*, 92–101.

Shimizu, T. (2009). Lipid mediators in health and disease: enzymes and receptors as therapeutic targets for the regulation of immunity and inflammation. Annu. Rev. Pharmacol. Toxicol. *49*, 123–150.

Suárez-Zamorano, N., Fabbiano, S., Chevalier, C., Stojanović, O., Colin, D.J., Stevanović, A., Veyrat-Durebex, C., Tarallo, V., Rigo, D., Germain, S., et al. (2015). Microbiota depletion promotes browning of white adipose tissue and reduces obesity. Nat. Med. *21*, 1497–1501.

Syed, I., Lee, J., Moraes-Vieira, P.M., Donaldson, C.J., Sontheimer, A., Aryal, P., Wellenstein, K., Kolar, M.J., Nelson, A.T., Siegel, D., et al. (2018). Palmitic

acid hydroxystearic acids activate GPR40, which is involved in their beneficial effects on glucose homeostasis. Cell Metab. *27*, 419–427.e4.

Takabatake, N., Sata, M., Inoue, S., Shibata, Y., Abe, S., Wada, T., Machiya, J., Ji, G., Matsuura, T., Takeishi, Y., et al. (2005). A novel polymorphism in secretory phospholipase A_2-IID is associated with body weight loss in chronic obstructive pulmonary disease. Am. J. Respir. Crit. Care Med. *172*, 1097–1104.

Taketomi, Y., Ueno, N., Kojima, T., Sato, H., Murase, R., Yamamoto, K., Tanaka, S., Sakanaka, M., Nakamura, M., Nishito, Y., et al. (2013). Mast cell maturation is driven via a group III phospholipase A_2-prostaglandin D_2-DP1 receptor paracrine axis. Nat. Immunol. *14*, 554–563.

Thomou, T., Mori, M.A., Dreyfuss, J.M., Konishi, M., Sakaguchi, M., Wolfrum, C., Rao, T.N., Winnay, J.N., Garcia-Martin, R., Grinspoon, S.K., et al. (2017). Adipose-derived circulating miRNAs regulate gene expression in other tissues. Nature *542*, 450–455.

Tian, C., Stokowski, R.P., Kershenobich, D., Ballinger, D.G., and Hinds, D.A. (2010). Variant in *PNPLA3* is associated with alcoholic liver disease. Nat. Genet. *42*, 21–23.

Titos, E., Rius, B., González-Périz, A., López-Vicario, C., Morán-Salvador, E., Martínez-Clemente, M., Arroyo, V., and Clària, J. (2011). Resolvin D1 and its precursor docosahexaenoic acid promote resolution of adipose tissue inflammation by eliciting macrophage polarization toward an M2-like phenotype. J. Immunol. *187*, 5408–5418.

Uhm, M., and Saltiel, A.R. (2015). White, brown, and beige; type 2 immunity gets hot. Immunity *42*, 15–17.

Uozumi, N., Kume, K., Nagase, T., Nakatani, N., Ishii, S., Tashiro, F., Komagata, Y., Maki, K., Ikuta, K., Ouchi, Y., et al. (1997). Role of cytosolic phospholipase A_2 in allergic response and parturition. Nature *390*, 618–622.

Uyama, T., Ichi, I., Kono, N., Inoue, A., Tsuboi, K., Jin, X.H., Araki, N., Aoki, J., Arai, H., and Ueda, N. (2012). Regulation of peroxisomal lipid metabolism by catalytic activity of tumor suppressor H-rev107. J. Biol. Chem. *287*, 2706–2718.

Vegiopoulos, A., Müller-Decker, K., Strzoda, D., Schmitt, I., Chichelnitskiy, E., Ostertag, A., Berriel Diaz, M., Rozman, J., Hrabe de Angelis, M., Nüsing, R.M., et al. (2010). Cyclooxygenase-2 controls energy homeostasis in mice by de novo recruitment of brown adipocytes. Science *328*, 1158–1161.

Vernochet, C., Peres, S.B., Davis, K.E., McDonald, M.E., Qiang, L., Wang, H., Scherer, P.E., and Farmer, S.R. (2009). C/EBPalpha and the corepressors CtBP1 and CtBP2 regulate repression of select visceral white adipose genes during induction of the brown phenotype in white adipocytes by peroxisome proliferator-activated receptor γ agonists. Mol. Cell. Biol. *29*, 4714–4728.

Villarroya, J., Flachs, P., Redondo-Angulo, I., Giralt, M., Medrikova, D., Villarroya, F., Kopecky, J., and Planavila, A. (2014). Fibroblast growth factor-21 and the beneficial effects of long-chain n-3 polyunsaturated fatty acids. Lipids *49*, 1081–1089.

Villarroya, F., Cereijo, R., Villarroya, J., Gavaldà-Navarro, A., and Giralt, M. (2018). Toward an understanding of how immune cells control brown and beige adipobiology. Cell Metab. *27*, 954–961.

von Allmen, C.E., Schmitz, N., Bauer, M., Hinton, H.J., Kurrer, M.O., Buser, R.B., Gwerder, M., Muntwiler, S., Sparwasser, T., Beerli, R.R., and Bachmann, M.F. (2009). Secretory phospholipase A_2-IID is an effector molecule of $CD4^+CD25^+$ regulatory T cells. Proc. Natl. Acad. Sci. USA *106*, 11673–11678.

Wang, B., Rong, X., Duerr, M.A., Hermanson, D.J., Hedde, P.N., Wong, J.S., Vallim, T.Q., Cravatt, B.F., Gratton, E., Ford, D.A., and Tontonoz, P. (2016). Intestinal phospholipid remodeling is required for dietary-lipid uptake and survival on a high-fat diet. Cell Metab. *23*, 492–504.

White, P.J., Arita, M., Taguchi, R., Kang, J.X., and Marette, A. (2010). Transgenic restoration of long-chain n-3 fatty acids in insulin target tissues improves resolution capacity and alleviates obesity-linked inflammation and insulin resistance in high-fat-fed mice. Diabetes *59*, 3066–3073.

Wolf, Y., Boura-Halfon, S., Cortese, N., Haimon, Z., Sar Shalom, H., Kuperman, Y., Kalchenko, V., Brandis, A., David, E., Segal-Hayoun, Y., et al. (2017). Brown-adipose-tissue macrophages control tissue innervation and homeostatic energy expenditure. Nat. Immunol. *18*, 665–674.

Wu, D., Molofsky, A.B., Liang, H.E., Ricardo-Gonzalez, R.R., Jouihan, H.A., Bando, J.K., Chawla, A., and Locksley, R.M. (2011). Eosinophils sustain adipose alternatively activated macrophages associated with glucose homeostasis. Science *332*, 243–247.

Yamamoto, K., Miki, Y., Sato, M., Taketomi, Y., Nishito, Y., Taya, C., Muramatsu, K., Ikeda, K., Nakanishi, H., Taguchi, R., et al. (2015). The role of group IIF-secreted phospholipase A_2 in epidermal homeostasis and hyperplasia. J. Exp. Med. *212*, 1901–1919.

Yan, Y., Jiang, W., Spinetti, T., Tardivel, A., Castillo, R., Bourquin, C., Guarda, G., Tian, Z., Tschopp, J., and Zhou, R. (2013). Omega-3 fatty acids prevent inflammation and metabolic disorder through inhibition of NLRP3 inflammasome activation. Immunity *38*, 1154–1163.

Zhao, M., and Chen, X. (2014). Eicosapentaenoic acid promotes thermogenic and fatty acid storage capacity in mouse subcutaneous adipocytes. Biochem. Biophys. Res. Commun. *450*, 1446–1451.

STAR★METHODS

KEY RESOURCES TABLE

REAGENT or RESOURCE	SOURCE	IDENTIFIER
Antibodies		
Goat anti-rabbit IgG (H+L) superclonal secondary antibody, Alexa Fluor 555	Thermo Fisher Scientific	Cat# A27039; RRID: AB_2536100
Rat anti-mouse F4/80 (clone Cl:A3-1)	Bio-Rad	Cat# MCA497GA; RRID: AB_323806
Rat anti-mouse CD206 (clone MR5D3)	Bio-Rad	Cat# MCA2235XZ; RRID: AB_324449
Rabbit anti-sPLA$_2$-IID polyclonal antibody	Miki et al., 2013	N/A
Rabbit polyclonal anti-UCP1	Abcam	Cat# ab10983; RRID: AB_2241462
Rabbit monoclonal anti-P-Akt (Ser473) (clone D9E)	Cell Signaling Technology	Cat# 4060; RRID: AB_2315049
Goat anti-rabbit IgG, Fc, HRP conjugate antibody	Millipore	Cat# AP156P; RRID: AB_91699
TruStain fcX (anti-mouse CD16/32) antibody	Biolegend	Cat# 101320; RRID: AB_1574975
APC anti-mouse/human CD11b (clone M1/70)	Biolegend	Cat# 101211; RRID: AB_312794
Anti-mouse CD11c PE (clone N418)	Thermo Fisher Scientific	Cat# 12-0114-81; RRID: AB_465551
FITC anti-mouse F4/80 (clone BM8)	Biolegend	Cat# 123107; RRID: AB_893500
Alexa Fluor 647 anti-mouse CD206 (MMR) (clone C068C2)	Biolegend	Cat# 141712; RRID: AB_10900420
CD45 monoclonal antibody FITC (clone 30-F11)	Thermo Fisher Scientific	Cat# 11-0451-81; RRID: AB_465049
FITC anti-mouse F4/80 (clone BM8)	Biolegend	Cat# 123107; RRID: AB_893500
PE rat anti-mouse Ly-6A/E (Sca-1) (clone D7)	BD PharMingen	Cat# 553108
Alexa Fluor 647 rat anti-mouse CD45R (B220) (clone RA3-6B2)	BD PharMingen	Cat# 557683
PE rat anti-mouse Ly-6G and Ly-6C (Gr1) (clone RB6-8C5)	BD PharMingen	Cat# 553128
Alexa Fluor 488 anti-mouse CD3ε (clone 145-2C11)	Biolegend	Cat# 100321, RRID: AB_389300
PE rat IgG2a, kappa isotype control antibody (clone RTK2758)	Biolegend	Cat# 400508; RRID: AB_326530
PE/Cy7 armenian hamster IgG isotype control antibody (HTK888)	Biolegend	Cat# 400907; RRID: AB_326593
PE rat IgG2b, kappa isotype control antibody (clone RTK4530)	Biolegend	Cat# 400508, RRID: AB_326530
Alexa Fluor 647 rat IgG2b, kappa isotype control antibody (clone RTK4530)	Biolegend	Cat# 400626; RRID: AB_389343
Chemicals, Peptides, and Recombinant Proteins		
Trizol reagent	Invitrogen	Cat# 15596026
Insulin solution	Sigma-Aldrich	Cat# I0516
Humalog	Eli Lilly	Cat# VL-7510
DAPI (4',6-Diamidino-2-phenylindole dihydrochloride)	Thermo Fisher Scientific	Cat# D1306
Collagenase D	Roche	Cat# 11088882001
Collagenase type II	Worthington	Cat# LS004176
Dispase II	Thermo Fisher Scientific	Cat# 17105041
Rosiglitazone	Sigma-Aldrich	Cat# R2408
CL316,243	Sigma-Aldrich	Cat# C5976
LPS	Sigma-Aldrich	Cat# L2654

(*Continued on next page*)

CellPress
OPEN ACCESS

Continued

REAGENT or RESOURCE	SOURCE	IDENTIFIER
Recombinant murine IFN-γ	PreproTech	Cat# 315-05
Leukoprol	Kyowa Kirin	Cat# 873399
Recombinant murine IL-4	PreproTech	Cat# 214-14
Recombinant murine IL-13	PreproTech	Cat# 210-13
Palmitic acid	Sigma-Aldrich	Cat# P0500
Linoleic acid	Cayman Chemicals	Cat# 60-33-3
Arachidonic acid	Cayman Chemicals	Cat# 506-32-1
α-Linolenic acid	Cayman Chemicals	Cat# 463-40-1
Eicosapentaenoic acid	Cayman Chemicals	Cat# 10417-94-4
Docosahexaenoic acid	Cayman Chemicals	Cat# 6217-54-5
9(S)-HODE	Cayman Chemicals	Cat# 73543-67-6
13(S)-HODE	Cayman Chemicals	Cat# 1176496-97-1
Eicosapentaenoic acid-d5	Cayman Chemicals	Cat# 10005056
1-heptadecanoyl-2-hydroxy-sn-glycero-3-phosphocholine (LysoPC17:0)	Avanti Polar Lipids	Cat# 855676
GSK137647	Tocris	Cat# 5257
AH7614	Tocris	Cat# 5256
Pioglitazone	Sigma-Aldrich	Cat# E6910
cOmplete mini protease inhibitor cocktail tablets	Roche	Cat# 11836153001
PhosSTOP phosphatase inhibitor cocktail tablets	Roche	Cat# 4906837001
MEMα	Wako	Cat# 135-15175
DMEM/F-12, GlutaMAX supplement	Thermo Fisher Scientific	Cat# 10565042
Critical Commercial Assays		
Mouse Insulin ELISA Kit	Morinaga	Cat# M1102
Mouse/Rat Leptin Quantikine ELISA Kit	R&D	Cat# MOB00
Mouse/Rat FGF-21 Quantikine ELISA Kit	R&D	Cat# MF2100
Transaminase CII-test Wako Kit	Wako	Cat# 431-30901
High Capacity cDNA Reverse Transcription Kit	Thermo Fisher Scientific	Cat# 4368814
TaqMan Gene Expression Master Mix	Thermo Fisher Scientific	Cat# 4369016
EnVision Detection System	Dako	Cat# K5007
Pierce BCA Protein Assay Kit	Thermo Fisher Scientific	Cat# 23227
ECL Prime western blotting detection reagent	GE Healthcare	Cat# RPN2232
RNeasy Lipid Tissue Mini Kit	QIAGEN	Cat# 74804
Experimental Models: Organisms/Strains		
Mouse: Floxed (exon 2, 3) *Pla2g2d* mice (*Pla2g2d*$^{f/f}$)	This paper	See Figure S4A
Mouse: B6.129P2-*Lyz2* $^{tm1(cre)Ifo}$/J	RIKEN	RBRC02302
Mouse: B6.Cg-*Lep* ^{ob}/J	The Jackson Laboratory	Cat# 00632; RRID: IMSR_JAX:000632
Mouse: *Pla2g4a*$^{-/-}$ mice	Uozumi et al., 1997	N/A
Oligonucleotides		
Primer/probe list for TaqMan Gene Expression Assay (see Table S1 for a full list)	This paper	See Table S1
Software and Algorithms		
FlowJo software v.10	TreeStar	https://www.flowjo.com/
Excel statistical program file yStat 2008	Igaku Tosho Shuppan	N/A
BZ-X Analyzer	KEYENCE	N/A
ImageJ	NIH	https://fiji.sc/

(*Continued on next page*)

Continued

REAGENT or RESOURCE	SOURCE	IDENTIFIER
MultiQuant software v.3	AB SCIEX	https://sciex.jp/products/software/multiquant-software
Other		
High Fat Diet 32	CLEA-Japan	Cat# HFD32
D12451 (Control diet)	Research Diet	See Table S2
D10020201 (ω3 PUFA-rich diet)	Research Diet	See Table S2
Medisafe mini	Terumo	Cat# GR-102

LEAD CONTACT AND MATERIALS AVAILABILITY

Further information and requests for resources and reagents should be directed to and will be fulfilled by the Lead Contact, Makoto Murakami (makmurak@m.u-tokyo.ac.jp). This study did not generate new unique reagents.

EXPERIMENTAL MODEL AND SUBJECT DETAILS

Mice

Global *Pla2g2d*$^{-/-}$ and *Pla2g2d*$^{fl/fl}$ mice were backcrossed onto a C57BL/6 genetic background (Japan SLC) for > 12 generations, and genotyping was performed on genomic DNA from tail biopsies by PCR (Miki et al., 2013). For conditional deletion of *Pla2g2d* in macrophages, *Pla2g2d*$^{fl/fl}$ mice were crossed with *Lys2-Cre* mice (Jackson Laboratory). Genotyping of conditional *Pla2g2d*$^{-/-}$ mice were performed using combined sets of sense primers 5′-agcacttgacacctgatgctgttccttctc-3′ or 5′-tagttggtgagcttc aggcta-3′ and an antisense primer 5′-ggacagattacagaggaggtcatggcatttc-3′ (Figure S4A). The PCR conditions were 95°C for 10 s and then 35 cycles of 95°C for 0 s and 65°C for 1 min on a Veriti Fast thermal cycler (Applied Biosystems), and the PCR products were analyzed by 1.5% (w/v) agarose gel electrophoresis with ethidium bromide. *Lep*$^{ob/ob}$ mice were obtained from Jackson Laboratory. *Pla2g4a*$^{-/-}$ mice were described previously (Uozumi et al., 1997). All mice were housed in climate-controlled (23°C) pathogen-free facilities with a 12 h light-dark cycle, with free access to standard LFD (CE-2; CLEA Japan) and water. All procedures involving animals were performed in accordance with protocols approved by the Institutional Animal Care and Use Committees of the University of Tokyo and Tokyo Metropolitan Institute of Medical Science under the Japanese Guide for the Care and Use of Laboratory Animals.

Culture of BMDMs

Mouse BM cells were cultured in MEMα medium (Wako) containing 10% (v/v) FBS, 100 U/ml penicillin and 100 μg/ml streptomycin supplemented with 100 ng/ml M-CSF (Leukoprol; Kyowa Kirin) to obtain BMDMs. The M-CSF-driven BMDMs were cultured for 12 h in serum-free medium (M0 macrophages) and then for 24 h in culture medium supplemented with 1 μg/ml LPS (Sigma-Aldrich) and 10 ng/ml IFN-γ (Peprotech) to induce M1 macrophages or with 20 ng/ml IL-4 (Peprotech) to induce M2 macrophages (Kadl et al., 2010). As required, following agents were added to the culture: 20 μM LA, AA, EPA or DHA, 10 μM 9(S)- or 13(S)-HODE (Cayman Chemicals), 100 μM palmitic acid (Sigma-Aldrich), 10 μM pioglitazone (PPARγ agonist) (Sigma-Aldrich), or 50 μM GSK137647 (GPR120 agonist) (Tocris).

Culture of primary adipocytes

Culture of primary adipocytes from sWAT was performed as described previously (Ohno et al., 2012). In brief, fat depots were digested in PBS containing 1.5 U/ml collagenase D (Roche) and 2.4 U/ml dispase II (Thermo Fisher Scientific) supplemented with 10 mM $CaCl_2$ at 37 C for 40-45 min. The primary cells were filtered through a 70-μm cell strainer and centrifuge at 500 g to collect SVF cells, which were then rinsed and plated on collagen coated plates. Adipocyte differentiation was induced by treating confluent cells in DMEM/F12 medium containing 10% FBS, 0.5 mM isobutylmethylxanthine, 125 nM indomethacin, 1 μM dexamethasone, 850 nM insulin, 1 μM rosiglitazone and 1 nM T3 (all from Sigma-Aldrich). Two days after induction, cells were switched to the maintenance medium containing 10% FBS, 850 nM insulin, 1 μM rosiglitazone and 1 nM T3. The differentiated cells were cultured for 24 h in lipid-depleted medium and then for 24 h in culture medium supplemented with 100 μM PUFAs (Cayman Chemicals) in the presence or absence of 100 μM AH7614 (GPR120 antagonist) (Tocris).

Ex vivo culture of WAT explants

Mouse sWAT was cultured in 1 mL of DMEM/F-12 medium containing 10% FBS, penicillin/streptomycin, and 2 mM GlutaMAX™ supplement (Thermo Fisher Scientific). After pretreatment with 100 μM EPA or vehicle for 2 h, the sWAT explants were cultured in the presence of 1 μM CL316,243 for 24 h.

CellPress
OPEN ACCESS

METHOD DETAILS

Quantitative RT-PCR

Total RNA was extracted from tissues using TRIzol reagent (Invitrogen). RNA was isolated from mouse tissues using the RNeasy Lipid Tissue Mini kit (QIAGEN). First-strand cDNA synthesis was performed using a High Capacity cDNA Reverse Transcriptase Kit (Applied Biosystems). PCR reactions were carried out using a TaqMan Gene Expression System (Applied Biosystems) on the ABI7300 and StepOnePlus Real Time PCR systems (Applied Biosystems). The probe/primer sets used are listed in Table S1.

Experiments using special diets

In the experiments for diet-induced obesity, global or macrophage-specific *Pla2g2d*-deficient mice and littermate control mice (8-wk-old, female) were placed on a HFD (High-fat diet 32; CLEA Japan) for up to 26 weeks, with those mice maintained on LFD (Rodent diet CE-2; CLEA Japan) as a control. In the rescue experiments, *Pla2g2d*$^{+/+}$ and *Pla2g2d*$^{-/-}$ mice were fed an ω3 PUFA-rich diet (D10020201; Research Diet) or lard-rich control diet (D12451; Research Diet) for up to 10 weeks. The composition of the ω3 PUFA-rich and control diets are shown in Table S2.

Adipocyte browning

For β_3-adrenergic stimulation, 8∼10-week-old female mice were treated intraperitoneally with the β_3-adrenergic agonist CL316,243 (1 mg/kg body weight, Sigma-Aldrich) once a day for 3 days. For cold stimulation, mice were placed at 30°C for 2 days and then at 4°C for appropriate periods in a temperature-controlled chamber (HC-10, Shin Factory). Rectal temperature was measured using an electronic thermometer (Physitemp Instruments). Expression of genes related to adipocyte browning and thermogenesis was evaluated by quantitative RT-PCR.

Glucose and insulin tolerance tests

Mice were fasted for 16 and 6 hours before intraperitoneally injection of glucose (2 mg glucose/g body weight) (Wako) and insulin (0.75 mIU/g body weight) (Eli Lilly) in saline, respectively. Blood glucose concentrations were monitored at various time intervals using a Medisafe-Mini blood glucose monitoring system (Terumo).

Oxygen consumption and locomotor activity

Oxygen consumption was measured every 3 min over 24 h under resting conditions using an MK-5000RQ metabolism measuring system for small animals (Muromachi Kikai). For measurement of basal locomotor activity, mice were placed into chambers of an ACTIMO-S food intake, drinking, and locomotor activity monitoring system (Shintechno). Food and water were provided *ad libitum*. Mice were allowed to acclimatize in the chambers for 24 h, and then their physical activities were measured over the next 24 h.

Immunoblotting

Tissues (100 mg) were soaked in 500 μL of RIPA buffer containing 50 mM Tris-HCl (pH 7.4), 150 mM NaCl, 0.1% (w/v) sodium deoxycholate, 0.1% SDS, 1 mM EDTA, 10 mM NaF, cOmplete protease inhibitors (Roche) and PhosSTOP phosphatase inhibitors (Roche), and then homogenized with a Precellys Evolution tissue homogenizer (Bertin). The homogenates (20 μg protein equivalents) were subjected to SDS-PAGE on 10% (w/v) gels under reducing conditions with 2-mercaptoethanol. Protein concentrations were determined with a BCA protein assay kit (Thermo Fisher Scientific) using bovine serum albumin (BSA; Sigma-Aldrich) as a standard. The separated proteins were electroblotted onto PVDF membranes (Millipore) with a semi-dry blotter (Transblot SD; Bio-Rad). After blocking with 5% (w/v) skim milk in 10 mM Tris-HCl (pH 7.4) containing 150 mM NaCl (TBS) and 0.1% (v/v) Tween 20 (TBS-T), the membranes were probed with rabbit antibody against Akt (C67E7; Cell Signaling) or phosphorylated Akt (p-Akt) Ser473 (D9E; Cell Signaling) at 1:1,000 dilution in TBS-T for 2 h, followed by incubation with horseradish peroxidase-conjugated anti-rabbit IgG (AP156P; Millipore) at 1:5,000 dilution in TBS-T for 2 h, and then visualized using the ECL Prime western blotting detection reagent (GE Healthcare). The signal intensities of p-Akt versus Akt were evaluated by densitometric analysis (Fusion Solo S; Vilber-Lourmat).

CT analysis

Mice were anesthetized with somnopentyl (0.5 mg/g body weight) (Kyoritsu Seiyaku) and their adiposity was analyzed using Latheta LCT-100 (Aloka).

Histology and immunohistochemistry

Mouse tissues were fixed with 100 mM phosphate buffer (pH 7.2) containing 4% (w/v) paraformaldehyde, embedded in paraffin, sectioned, mounted on glass slides, deparaffinized in xylene, and rehydrated in ethanol with increasing concentrations of water. Hematoxylin and eosin staining was performed on the 5-μm-thick cryosections, and the stained sections were analyzed using a

BZ-X710 microscope (Keyence). Expression of UCP1 protein was assessed by immunostaining of deparaffinized WAT sections using rabbit polyclonal antibody against mouse UCP1 (ab10983, Abcam) and an EnVision™ Detection System (Dako).

Whole mount immunofluorescence microscopy of adipose tissue

Mouse WAT was fixed with 100 μL of 4% (w/v) paraformaldehyde for 3 h in a 96-well plate, washed with PBS, and treated with 200 μL of 0.4% (v/v) Triton X-100 (Sigma) in PBS overnight at room temperature for permeabilization. After washing, the tissue was incubated with 100 μL of 5% (w/v) BSA in PBS (PBS-BSA) for blocking. After washing with PBS, the tissue was treated with rabbit anti-mouse PLA2G2D antibody (Miki et al., 2013) in PBS-BSA (1:400 dilution) at 4°C overnight, washed, and then treated with Alexa Fluor 555-conjugated goat anti-rabbit IgG (A27039, Thermo Fisher Scientific) in PBS-BSA (1:400 dilution) for 2 h at room temperature. After washing with PBS, the tissue was treated with rat anti-mouse F4/80 antibody (MCA497GA, Bio-Rad) or anti-mouse CD206 antibody (MCA2235XZ, Bio-Rad) in PBS-BSA (1:100 dilution) at 4°C overnight, washed, and then incubated with FITC-conjugated anti-rat IgG (F6258, Sigma-Aldrich) in PBS-BSA (1:400 dilution) for 2 h at room temperature. After washing, the tissue was counterstained with 4′,6-diamidine-2′-phenylindole dihydrochloride (DAPI) (5 μg/ml) for 10 min, washed, and then analyzed using a confocal laser microscopy (A1 HD25; Nikon).

Isolation of SVF

Adipose tissues were excised and minced in Hank's solution with 0.5% (w/v) BSA. After centrifugation at 800*g* for 5 min, the floating pieces of adipose tissue were incubated at 37°C for 30 min in 1 mg/ml collagenase type II (Worthington) in Hank's solution with shaking. The suspension was filtered through a 70-μm cell strainer (BD Biosciences) and then centrifuged at 800*g* for 5 min to separate floating adipocytes from the SVF pellet. After washes, the SVF pellet was suspended in red blood cell-lysing buffer and incubated for 5 min on ice.

Flow cytometry

The isolated SVF cells were incubated with TruStain fcX (anti-mouse CD16/32) (BioLegend) for blocking, incubated with either labeled monoclonal antibody or isotype control antibody (hamster IgG (HTK888), rat IgG_{2a} (RTK2758) or rat IgG_{2b} (RTK4530); BioLegend), and analyzed by flow cytometry with a FACSAria III (BD Biosciences) and FlowJo (Tree Star) software. The antibodies used were specific for mouse F4/80 (BM8, BioLegend), CD11b (M1/70, BioLegend), CD11c (N418, Thermo Fisher Scientific), CD206 (C068C2, BioLegend), Sca1 (D7, BD PharMingen), CD45 (30-F11, Thermo Fisher Scientific), CD11b (M1/70, Biolegend), B220 (RA3-6B2, BD PharMingen), and Ly6G (Gr1) (RB6-8C5, BD PharMingen).

Measurement of serum markers

Serum insulin and leptin levels were quantified by a mouse insulin ELISA kit (Morinaga) and a leptin immunoassay kit (R&D Systems), respectively. Serum ALT levels were quantified using the transaminase CII-test Wako kit (Wako). Plasma FGF21 levels were determined using Mouse/Rat FGF-21 Quantikine ELISA Kit (R&D Systems). Analysis of plasma lipoproteins was performed by LipoSearch (Skylight Biotech).

Lipidomics analysis

Lipidomics (ESI-MS) was performed in accordance with our current protocol (Miki et al., 2013; Yamamoto et al., 2015). In brief, for detection of phospholipids, tissues were soaked in 10 volumes of 20 mM Tris-HCl (pH 7.4) and homogenized with a Polytron homogenizer. Lipids were extracted from the homogenates by the method of Bligh and Dyer (Yamamoto et al., 2015). MS analysis was performed using a 4000Q-TRAP quadrupole-linear ion trap hybrid mass spectrometer (AB Sciex) with liquid chromatography (LC; NexeraX2 system; Shimazu). The samples were applied to a Kinetex C18 column (1 × 150 mm i.d., 1.7 μm particle) (Phenomenex) coupled to ESI-MS/MS. The samples injected by an autosampler (10 μl) were separated by a step gradient with mobile phase A (acetonitrile/methanol/water = 1:1:1 [v/v/v] containing 5 μM phosphoric acid and 1 mM ammonium formate) and mobile phase B (2-propanol containing 5 μM phosphoric acid and 1 mM ammonium formate) at a flow rate of 0.2 ml/min at 50°C. For detection of fatty acids and their oxygenated metabolites, tissues were soaked in 10 volumes of methanol and then homogenized with a Polytron homogenizer. After overnight incubation at −20°C, water was added to the mixture to give a final methanol concentration of 10% (v/v). The samples in 10% methanol were applied to Oasis HLB cartridges (Waters), washed with 10 mL of hexane, eluted with 3 mL of methyl formate, dried under N_2 gas, and dissolved in 60% methanol. The samples were then applied to a Kinetex C18 column (1 × 150 mm i.d., 1.7 μm particles) (Phenomenex) coupled to ESI-MS/MS as described above. The samples injected by an autosampler (10 μl) were separated using a step gradient with mobile phase C (water containing 0.1% (v/v) acetic acid) and mobile phase D (acetonitrile/methanol = 4:1; v/v) at a flow rate of 0.2 ml/min at 45°C. Identification was conducted using multiple reaction monitoring (MRM) transition and retention times, and quantification was performed based on the peak area of the MRM transition and the calibration curve obtained with an authentic standard for each compound. As internal standards, *d5*-labeled EPA (1 nmol; Cayman Chemicals) and LPC17:0 (1 nmol; Avanti Polar Lipids) were added to each sample.

CellPress
OPEN ACCESS

QUANTIFICATION AND STATISTICAL ANALYSIS

All values are given as the mean ± SEM. Differences between two groups were assessed by using the unpaired two-tailed t test or ANOVA Dunnett's test using the Excel Statistical Program File yStat 2008 (Igaku Tosho Shuppan, Tokyo, Japan). Differences at *P values* of less than 0.05 were considered statistically significant.

DATA AND CODE AVAILABILITY

The microarray data can be accessed at the GEO accession number GSE56038 (Sato et al., 2014).